Inverse Tsunami Flow Modeling Including Nonequilibrium Sediment Transport, With Application to Deposits From the 2011 Tohoku-Oki Tsunami

AUTHOR(S):

Naruse, Hajime; Abe, Tomoya

CITATION:

Naruse, Hajime ...[et al]. Inverse Tsunami Flow Modeling Including Nonequilibrium Sediment Transport, With Application to Deposits From the 2011 Tohoku-Oki Tsunami. Journal of Geophysical Research: Earth Surface 2017, 122(11): 2159-2182

ISSUE DATE:

2017-11

URL:

http://hdl.handle.net/2433/228311

AGU PUBLICATIONS
JGR
Journal of Geophysical Research: Earth Surface

RESEARCH ARTICLE
10.1002/2017JF004226

Key Points:
- Inverse model of tsunamis from spatial variation of thickness and grain size distribution of deposits along 1-D transect is proposed
- The model reconstructs flow depths and velocities as well as sediment concentrations during tsunamis
- The model is suitable for analysis of ancient tsunami deposits

Correspondence to:
H. Naruse,
naruse@kueps.kyoto-u.ac.jp

Citation:
Naruse, H. & Abe, T. (2017). Inverse tsunami flow modeling including nonequilibrium sediment transport, with application to deposits from the 2011 Tohoku-Oki tsunami. *Journal of Geophysical Research: Earth Surface*, *122*, 2159–2182. https://doi.org/10.1002/2017JF004226

Received 20 JAN 2017
Accepted 9 OCT 2017
Accepted article online 18 OCT 2017
Published online 10 NOV 2017

Inverse Tsunami Flow Modeling Including Nonequilibrium Sediment Transport, With Application to Deposits From the 2011 Tohoku-Oki Tsunami

Hajime Naruse[1] **and Tomoya Abe**[2]

[1]Division of Earth and Planetary Sciences, Graduate School of Science, Kyoto University, Kyoto, Japan, [2]Research Institute of Geology and Geoinformation, Geological Survey of Japan, Tsukuba, Japan

Abstract Tsunami deposits provide important clues to understand ancient tsunami events. Several inverse models have been proposed to estimate the magnitude of paleotsunamis from their deposits. However, existing models consider neither nonuniform transport of suspended sediment nor turbulent mixing, which are essential factors governing sedimentation from suspension in tsunami flows. Here we propose a new inverse model of tsunami deposit emplacement, considering both transport of nonuniform suspended load and entrainment of basal sediments. This inversion model requires the spatial distribution of deposit thickness and the pattern of grain size distributions of the tsunami deposit along a 1-D shoreline-normal transect as input data. It produces as output run-up flow velocity, inundation depth, and concentration of suspended sediment. To solve for advection of nonuniform suspended load, a transformed coordinate system is adopted, which increases computational efficiency. Tests of model inversions using artificial data successfully allow reconstruction of the original input values, suggesting the effectiveness of our optimization method. We apply our new inversion model to the 2011 Tohoku-Oki tsunami deposit on Sendai Plain, Japan. The thickness and grain size distribution of the tsunami deposit was measured along a 4 km long transect normal to the coastline. The result of our inversion fits well with the observations from aerial videos and field surveys. We conclude that this method is suitable for the analysis of ancient tsunami deposits and that it has the advantage of requiring relatively little information about the condition of the emplacing paleotsunami for reconstruction.

Plain Language Summary This paper proposes a method to estimate flow conditions of past tsunamis from their deposits. The method is useful for evaluating hazard risks from geologic records.

1. Introduction

Tsunamis represent one of the most serious natural hazards. However, risk assessment of this hazard is impeded by the difficulty of observation of the event itself. In many regions the recurrence interval of tsunamis often exceeds the time scale of historic records. Estimates of the frequency and magnitudes of prehistoric tsunamis help fill this gap. From this viewpoint, tsunami deposits have been studied in order to understand the ancient tsunamis that created them (Atwater, 1987; Minoura et al., 2001). Tsunamis can cause immense amounts of sediment transport and deposition near coastal areas and forms sedimentary layers known as tsunami deposits. Research on tsunami deposits can provide useful information about the occurrence of past tsunamis and can aid in the estimation of their recurrence intervals, knowledge of which is helpful for future risk assessment of tsunami hazards (Goff et al., 2012). Tsunami deposits on coastal lowlands are especially useful, because the preservation potential of the deposits is relatively high, and the influence of local topography is often minimal in such regions. The study of tsunami deposits enable us to expand our knowledge of tsunamis into the time before written records were kept.

In addition to recurrence intervals, estimates of typical magnitude of flow velocity and depth of inundation are essential for planning for disaster prevention due to tsunamis. For instance, a knowledge of the inundation depth of past tsunamis is needed in order to design coastal levees. With this in mind, several inverse models of tsunami deposits have been proposed to estimate the magnitude of paleotsunamis (Jaffe et al., 2016).

There are two types of inverse models of the tsunami deposits: the point and 1-D line models (Jaffe et al., 2016). Point models such as Moore et al. (2007), Jaffe and Gelfenbaum (2007), or Naruse et al. (2012) consider flow

properties from input data of the tsunami deposits at a single location, whereas the 1-D line models such as Soulsby et al. (2007) or Tang and Weiss (2015) reconstruct the behavior of the tsunami from data of the tsunami deposit collected at multiple sampling points on a transect normal to the shoreline. Two-dimensional models are potentially possible, but they have not been proposed.

Point models have an advantage in regard to ease to collect data from the deposit, but the models are strongly limited in their applications. Deposition is a process caused by spatially nonuniform sediment transport as captured by the Exner equation (Kneller, 1995). The sedimentation rates are decided by the spatial differentiation of sediment transport rates. Even if the flow velocities and other properties at a certain point are the same, erosion occurs where the sediment transport rate is increasing, and deposition occurs where the transport rate is decreasing. The depositional processes considered here depend on the spatial distribution of volume of transported sediments, so that reconstruction of the flow conditions from a single locality is possible only when a specific condition is achieved. Jaffe and Gelfenbaum (2007) proposed the point model TsuSedMod which analyzes the pattern of normal grading in tsunami deposits, assuming that the deposits have settled from suspended sediments obeying the Rouse concentration profile. Temporal variation of deceleration of the flow is not considered in this model, so that the calculated result of deposition is essentially similar to the assumption in which deposition occurs only in the stagnant phase after run-up. Sediment concentration is assumed to be uniform along a streamwise direction, and thus a sediment flux exceeding the capacity of suspension from upstream need not be supposed. Because of this model assumption, application of TsuSedMod should be limited to study sites situated in areas where the run-up flow is expected to approach the condition of uniform steady flow. Results of inversions using TsuSedMod strongly depends on identification of the line of division demarcating the lower part of the deposit emplaced by run-up flow itself and the upper part emplaced by subsequent stagnant flow. If the division formed from nonuniform suspension transport is included in this analysis, very high flow velocity is typically estimated. Indeed, Choowong et al. (2008) reported that TsuSedMod estimates extremely high flow velocities of the 2004 Indian Ocean tsunami on Phuket, Thailand as 19–21 m/s at a location corresponding to 30 m landward from the shoreline. This model also requires information on the inundation depth, which is rarely available in cases of paleotsunami deposits.

On the other hand, estimates of the critical velocity of motion of sediment particles have been commonly used for the estimation of flow velocity from the deposits (Choowong et al., 2008; Komar, 1985; Kubo et al., 1998; Naruse et al., 2012). This kind of analysis can be regarded as another type of point inversion model. For example, Naruse et al. (2012) estimated that the run-up velocity of the 2011 Tohoku-Oki tsunami on Rikuzentakata City was at least in the range from 2.4 to 2.7 m/s on the basis of the critical velocity for the bedload motion of the largest grain size in the tsunami deposit. In this analysis, the exposure (hiding) effect associated with multiple grain sizes was considered in estimating the incipient motion of sediment particles. Also, Moore et al. (2007) analyzed the 1929 Newfoundland tsunami deposit in terms of the critical velocity for particles to be suspended. These methods using critical velocity, however, provide only estimates of minimum values of flow velocity, because deposition can occur even at velocities higher than the threshold of particle motion when the volume flux of supplied sediment exceeds the capacity of sediment transport at the site in question.

On the one hand, 1-D line models are superior to point models because they are applicable to nonequilibrium conditions. However, they require larger efforts for data acquisition than point models. A simple 1-D line model has been proposed by Soulsby et al. (2007); it was used to reconstruct the conditions of both the 1929 Newfoundland tsunami on Taylor Bay and the ancient tsunami in Fullerton, Scotland. These were rather small scale as compared to the 2011 Tohoku-Oki tsunami considered here. As described in the previous section, the model of Soulsby et al. (2007) assumes that no turbulent mixing occurs in the flow and that all sediment settles out during the run-up flow. This "moving settling column" model supposes that sediments are suspended uniformly in a water column and are transported inland until the finest sediment particle at the top of the water column settles to the bottom. Judging from the model assumptions, the applicability of their method should be limited to the cases for which flow velocity is relatively small. Higher flow velocities (and thus higher bed shear stresses) cause both strong turbulent mixing and sediment entrainment, conditions at which their model assumptions cannot be justified. Much larger tsunamis such as the Tohoku-Oki event considered here have inundated as much as several hundreds of meters inland; the relatively well-documented Tohoku-Oki event, in particular, showed very high velocities. Such large-scale run-up flows are out of the scope of the method of Soulsby et al. (2007). In fact, Sugawara (2014) reported a large discrepancy in the distribution of sand deposits between the predictions of Soulsby et al. (2007) and observations. In the case of Sendai Plain, medium sand reaches 2,500 m inland (Figure 9), so that their model predicts that the

flow velocity must exceed 24 m/s at the flow height of 5 m, whereas the observed flow velocity is 6.9 m/s at maximum. Settling advection models such as Moore et al. (2007) or Woodruff et al. (2008) also neglect turbulent mixing processes in tsunamis, so that their application should be limited to small-scale tsunamis.

To summarize, the strongly nonequilibrium assumption of Soulsby et al. (2007) sharply contradicts that of Jaffe and Gelfenbaum (2007), so that these two models should be applied only to situations appropriate to the model itself. Another 1-D line inverse model, TSUFLIND, reconstructs the behavior of tsunamis based on the shallow-water equations (Tang & Weiss, 2015). It is of notable value that the model incorporates hydrodynamics of tsunamis. In so far as the model employs both TsuSedMod and Soulsby et al.'s model as components in the prediction of depositional processes, however, this model shares limitations of applicability with these two models.

To remove these restrictions, we propose a new inverse model named FITTNUSS (Framework of Inversion of Tsunami deposits considering Transport of Nonuniform Unsteady Suspension and Sediment entrainment), whose implementation is provided as the open source software written in Python (http://turbidite.secret.jp/python/FITTNUSS/). The model proposed in this study is classified as a 1-D line model. Turbulent mixing, resuspension from basal active layer and advective transport of suspension are incorporated in this model, although flow dynamics is simplified to the quasi-steady condition. In addition, damping of turbulence caused by density stratification due to suspended sediment itself is also incorporated in a form allowing computational efficiency. The generality of the physics embedded in this model suggests wider applicability to a range of situations, as illustrated below. Indeed, we apply our model to the 2011 Tohoku-Oki tsunami deposit without any parametric calibration and obtain reasonable estimations of run-up flow velocity and the inundation depth using only measurements of the tsunami deposit along a 4 km transect normal to the shoreline.

2. Forward Model Description

Here we describe the forward model used in the inverse model FITTNUSS. This model is based on the layer-averaged shallow-water equations, although they are simplified in order to treat the hydraulics of tsunamis. The model calculates the spatial variation of the thickness and grain size distribution of the tsunami deposit from input values of (1) maximum distance of horizontal run-up, (2) maximum inundation depth, (3) run-up velocity, and (4) sediment concentration of each grain size class.

2.1. Flow Dynamics and Sediment Transport

Tsunami inundation flow onto dry land is considered. Flow properties in the alongshore direction are taken to be constant (1-D approximation). Generally, tsunamis erode coastal areas and aeolian dunes, and deposit sediments in inland regions (Naruse et al., 2012). The upstream (seaward) bound of the calculation domain is set at the downstream (landward) bound of erosional region in this model. Our model thus assumes only deposition or bypassing of sediment within the calculational domain (Figures 1 and 2), while resuspension from basal sediment deposited from the tsunami may occur. Therefore, in this model all of the suspended load contained in the tsunami is derived from outside of the calculation domain. Bedload sediment transport is not considered in this model. The tsunami inundation flow can exchange suspended load with noncohesive sediment on the bed; however, the antecedent land surface is assumed to be nonerodible.

Flow dynamics of tsunamis are approximated by layer-averaged one-dimensional equations as follows (Figure 2):

$$\frac{\partial h}{\partial t} + \frac{\partial Uh}{\partial x} = 0, \tag{1}$$

$$\frac{\partial Uh}{\partial t} + \frac{\partial U^2 h}{\partial x} = ghS - \frac{1}{2}g\frac{\partial h^2}{\partial x} - u_*^2. \tag{2}$$

where t is time and x is a bed-attached streamwise coordinate that is transverse to the shoreline and is positive landward (downstream). Here tsunami flow thickness (inundation depth) is denoted as h and flow velocity is denoted as U. In addition, g denotes gravitational acceleration, S denotes bed slope, and u_* denotes friction velocity ($u_* = \sqrt{\tau_b/\rho_f}$, where τ_b and ρ_f are bed shear stress and density of water). Sediment conservation in tsunamis takes the form:

$$\frac{\partial C_i h}{\partial t} + \frac{\partial UC_i h}{\partial x} = w_{si}(F_i E_{si} - r_{0i} C_i). \tag{3}$$

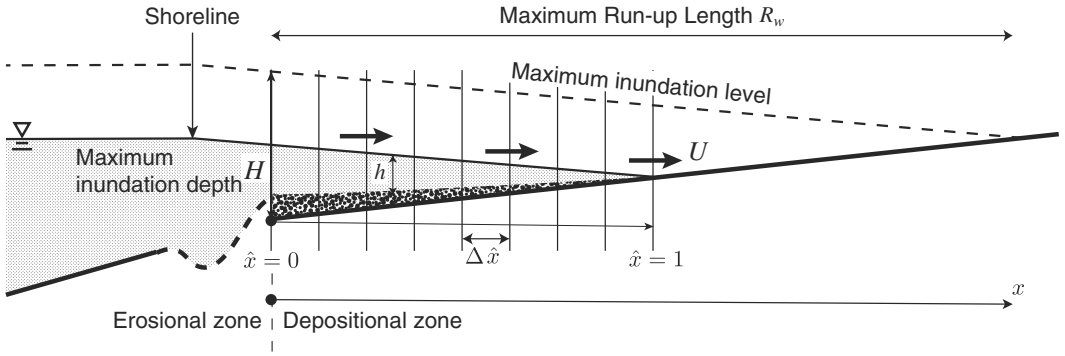

Figure 1. Explanation of model configuration. This figure illustrates an intermediate time step in the calculation. The velocity of tsunami run-up U is assumed to be constant in time and space. The inundation depth h increases in time at a constant rate until it reaches its maximum value H at the seaward (upstream) boundary. The maximum horizontal run-up distance is defined as R_w, and the water surface slope is taken to be constant ($\partial h/\partial x = -H/R_w$). The upstream (seaward) boundary of the calculation domain is set at the downstream (landward) boundary of the erosional region in this model. The bed-attached streamwise coordinate x is set transverse to the shoreline and is positive landward (downstream). A transformed coordinate system is introduced for numerical solution in this study, within which the moving front edge of the tsunami is located at a fixed value of the dimensionless spatial coordinate $\hat{x} = 1$.

where the grain size distribution of sediment is discretized to n grain size classes, with C_i denoting the volume concentration in suspension of the ith grain size class and total concentration summed over all grain size ranges $C_t = \sum C_i$. The symbols w_{si}, E_{si}, and r_{0i} indicate settling velocity, sediment entrainment coefficient and ratio of near-bed to layer-averaged concentration of the ith grain size class, respectively. Finally, F_i denotes the volumetric fraction of sediment particles in the ith grain size class in the bed surface active layer above the

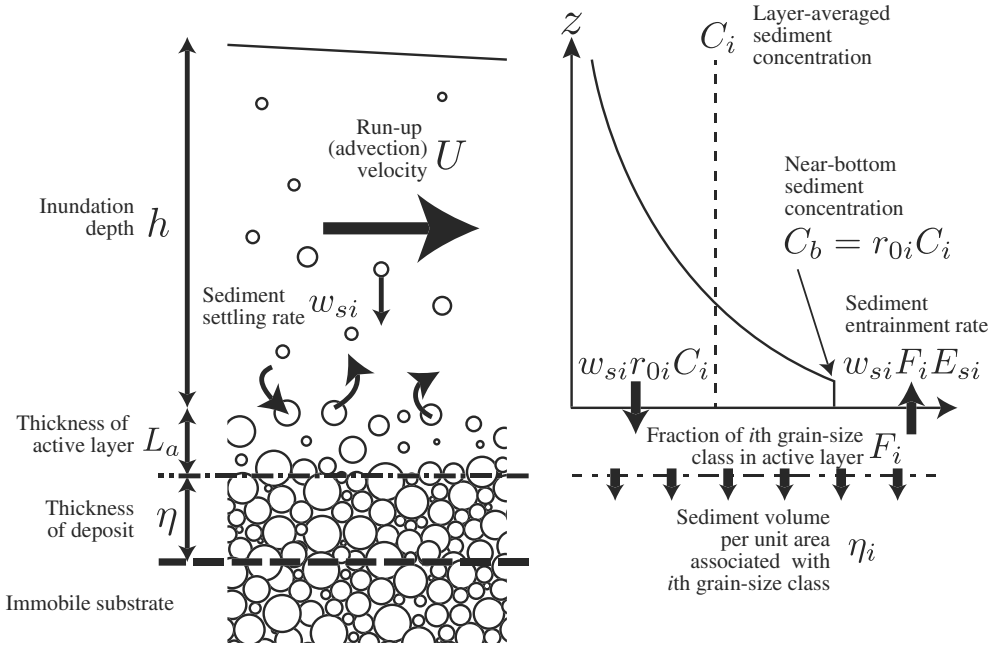

Figure 2. Explanation of model parameters. The layer-averaged sediment concentration of the ith grain size class is defined as C_i. Suspended sediment is transported at the constant velocity U in the run-up flow of the tsunami. The run-up flow exchanges suspended sediment with the active layer (L_a in thickness) on the top of the tsunami deposit (η in thickness) by settling and entrainment. The volumetric rate of settling of the ith grain size class of sediment is calculated from the basal sediment concentration $r_{0i}C_i$ multiplied by the sediment settling velocity w_{si}. The sediment entrainment rate from the active layer is $w_{si}F_iE_{si}$, where F_i is the volumetric fraction of the ith grain size class in the active layer and E_{si} is the unit dimensionless rate of sediment entrainment. The time variation of grain size distribution in the active layer is computed in this model.

substrate. Here it is assumed that suspended sediment exchanges only with the bed sediment in this active layer (Hirano, 1971).

Equations (1)–(3) are the layer-averaged equations of balance of fluid mass, momentum, and sediment mass. The first term on the right-hand side of equation (2) is the gravity force toward the downcurrent direction, and the second and third terms denote water pressure and frictional forces, respectively. The term on the right-hand side of equation (3) indicates that suspended load in the flow varies depending on the balance between sediment entrainment from the active layer of the bed surface and particle settling from the basal part of the flow.

2.2. Sedimentation From Tsunamis

Let η denote bed thickness and η_i denote the volume per unit area (thickness) of sediments of the ith grain size class including porosity. The Exner equation of bed sediment continuity of the ith grain size class can be written in the form:

$$\frac{\partial \eta_i}{\partial t} = \frac{1}{1-\lambda_p} w_{si}(r_{0i}C_i - F_i E_{si}). \tag{4}$$

where λ_p is the porosity of the bed sediment. Equation (4) predicts mass balance based on the volumetric sedimentation rate of each grain size class from suspension. The total sedimentation rate is expressed as follows:

$$\frac{\partial \eta}{\partial t} = \sum \frac{\partial \eta_i}{\partial t}. \tag{5}$$

The above equations require fractions F_i of each of the ith grain size class in the active layer in order to calculate exchange between suspension and bed material. The time variation of grain size distribution in the active layer caused by sedimentation can be written in the form (Hirano, 1971)

$$L_a \frac{\partial F_i}{\partial t} = \frac{\partial \eta_i}{\partial t} - F_i \frac{\partial \eta}{\partial t}, \tag{6}$$

where L_a denotes thickness of the active layer.

After the flooding flow of the tsunami becomes stagnant, it is assumed that all suspended sediment in the water column settles out. Thus, the duration of the stagnant phase of the tsunami T_{stag} is assumed to be larger than h/w_{sF} in this model, where w_{sF} corresponds to the fall velocity of the finest size class. In this case, the volume of the final deposit of the ith grain size class per unit area η_{fi} is obtained as follows:

$$\eta_{fi} = \eta_i\big|_{t=T_{inu}} + \frac{h\, C_i\big|_{t=T_{inu}}}{1-\lambda_p} \tag{7}$$

where T_{inu} is time for the inundation flow to reach the maximum run-up point. Thus, tsunamis in this model can entrain and deposit sediment throughout the run-up phase, and sediment in the water column can continue to deposit during the stagnant phase.

2.3. Closures for Equations of Flow Dynamics and Sediment Transport

An evaluation of the friction velocity u_* is required to close equations (1)–(3). For clear water flows, the following relation is generally assumed:

$$u_* = \sqrt{C_f} U \tag{8}$$

where C_f is a dimensionless friction coefficient. In this study the friction coefficient is defined in terms of the corresponding value of Manning's coefficient $n(= 0.03)$ that is frequently used for numerical simulations of tsunamis. The relationship between two parameters C_f and n takes the form

$$n = h^{\frac{1}{6}} \sqrt{\frac{C_f}{g}} \tag{9}$$

The thickness of the active layer L_a is obtained from the empirical function proposed by Yoshikawa and Watanabe (2008). They suggest that the thickness of the active layer exchanging with suspended sediment on a flat bed can be reasonably approximated by

$$L_a = \frac{D_m \tau_{*m}}{C_q \tan\theta} \tag{10}$$

where D_m denotes the mean grain size in the active layer and τ_{*m} denotes the Shields dimensionless shear stress for the mean grain size D_m computed as

$$\tau_{*m} = \frac{u_*^2}{RgD_m} \tag{11}$$

In addition, C_q and θ denote sediment concentration in the active layer and internal frictional angle of sediment particles, respectively. In this study, the values 0.1 and 0.5236 are respectively given for C_q and θ on the basis of Yoshikawa and Watanabe (2008). The parameter R denotes submerged specific density of sediment particles ($R = 1 - \rho_s/\rho_f$ where ρ_s is density of sediment particles).

Relations for settling velocity w_{si}, sediment entrainment coefficient E_{si}, and concentration ratio r_{0i} are required for closure of the model. These parameters are obtained from relations involving grain diameter D_i and other flow parameters. For settling velocity w_{si}, we employed the empirical relation of Dietrich (1982) as follows:

$$\frac{w_{si}}{\sqrt{RgD_i}} = \exp\left\{-a_1 + a_2\log(Re_{pi}) - a_3[\log(Re_{pi})]^2 - a_4[\log(Re_{pi})]^3 + a_5[\log(Re_{pi})]^4\right\} \tag{12}$$

where Re_{pi} is the particle Reynolds number defined as

$$Re_{pi} = \frac{\sqrt{RgD_i}D_i}{\nu}. \tag{13}$$

Here ν is kinematic viscosity of water. The parameters a_1, a_2, a_3, a_4, and a_5 are empirical constants. The parameter E_{si} can be estimated with the following empirical fit (van Rijn, 1984):

$$E_{si} = 0.015\frac{D_{50}}{a}\frac{T_i^{1.5}}{Re_{pi}^{0.2}} \quad \text{with} \quad E_{si} < 0.05 \tag{14}$$

where D_{50} is median grain size of bed sediment and a denotes a reference level that is defined as half of the bed roughness value k_s, with a minimum value of 0.01 m. T_i is dimensionless bed-shear stress parameter defined as

$$T_i = \frac{{u_{*i}}^2}{u_{*ci}^2} - 1 \tag{15}$$

where u_{*ci} is the critical friction velocity of sediment particles in the ith grain size class.

The initial bed is nonerodible in our model, and therefore, sediment entrainment from the initial bed ($\eta = 0$) is suppressed as follows:

$$E_{si} = \frac{r_{0i}C_i}{F_i} \ (\eta = 0) \tag{16}$$

Assuming a Rouse-type equilibrium profile of sediment concentration (Rouse, 1937), the ratio r_{0i} of near-bed to layer-averaged sediment concentration of the ith grain size class takes the form

$$r_{0i} = 1 \Big/ \int_{0.05}^{1} \left(\frac{1-\xi}{19\xi}\right)^{2.5\mu_i} d\xi \tag{17}$$

where $\xi = z/h$ and

$$\mu_i = \frac{w_{si}}{u_*} + \frac{\psi_i}{\kappa} \tag{18}$$

Here κ denotes the Karman constant (0.4). Coefficient ψ_i corrects for the effect of damping of turbulence in the flow due to density stratification caused by suspended sediment (van Rijn, 1984):

$$\psi_i = 2.5\left(\frac{w_{si}}{u_*}\right)^{0.8}\left(\frac{\sum r_{0i}C_i}{1-\lambda_p}\right)^{0.4} \tag{19}$$

Equation (17) can be approximated by the following relation:

$$r_{0i} = b_1 + b_2\mu_i^{b_3}, \tag{20}$$

where b_1, b_2, and b_3 denote curve fit parameters obtained by the least squares fit to equation (17), taking the values 1.16, 7.9, and 1.59, respectively. Because equation (19) contains the term $r_{0i}C_i$, equation (20) becomes an implicit function of r_{0i}. Therefore, an iterative scheme is needed to obtain the solution of equation (20).

2.4. Simplification of Fluid Dynamics of Tsunamis

We employed the scheme to simplify the hydrodynamics of tsunamis proposed by Soulsby et al. (2007), because the computational efficiency of the numerical solutions of (1)–(3) is needed in an iterative calculation. In this scheme, the water surface of a tsunami is approximated as linear, which means that the flow depth of the tsunami h decreases linearly with distance x. The increase rate of water level in the inundation phase of a tsunami is assumed to be constant, so that the flow depth h increases linearly with time t. The run-up flow velocity U is uniform in time and space. Defining the maximum horizontal run-up distance as R_w, the time T_{inu} to reach the maximum run-up point is given as

$$T_{inu} = \frac{R_w}{U}. \tag{21}$$

The imposed linear increase of both the run-up point and flow depth implies that the gradient of flow height $\partial h/\partial x$ is constant in time and space:

$$\frac{\partial h}{\partial x} = -\frac{H}{R_w} \tag{22}$$

where H denotes the maximum run-up depth at the location $x = 0$.

Integration of equation (1) with equation (22) yields

$$h = \frac{H}{R_w}(Ut - x). \tag{23}$$

Equation (23) is valid only when $Ut > x$; otherwise, $h = 0$.

Finally, equation (3) with equation (23) can be recast in the form

$$\frac{\partial C_i}{\partial t} + U\frac{\partial C_i}{\partial x} = \frac{R_w}{H(Ut-x)}\left\{w_{si}\left(F_iE_{si} - r_{0i}C_i\right)\right\}. \tag{24}$$

According to the model assumptions described above, the velocity of the run-up flow of the tsunami is uniform and steady, but the inundation depth varies in time and space. Therefore, this model simplification is called herein as the quasi-steady flow assumption.

2.5. Nondimensionalization and Coordinate Transformation

Equation (24) could be solved numerically so yielding predictions for temporal and spatial variation of suspended sediment in tsunamis. It should be noted, however, that (a) high flow velocity U in the advective term on the left-hand side of the equation and (b) the necessity of imposing a boundary condition at $x = Ut$ disturb the stability and computational efficiency of typical numerical schemes. Therefore, a transformed coordinate system is applied to equation (24).

The tsunami flooding flow has downstream propagating boundary (corresponding to the inundation limit of the tsunami). To treat this boundary condition, a deforming grid approach is employed, and the moving boundary is fixed by means of a Landau transformation as follows (Crank, 1984):

$$\hat{x} = \frac{x}{Ut} = \frac{x}{UT_{inu}\hat{t}} \tag{25}$$

where $\hat{x}$ is a dimensionless spatial coordinate and the front edge of the tsunami is at the fixed point $\hat{x} = 1$. Time t is also nondimensionalized as follows:

$$\hat{t} = \frac{t}{T_{\mathrm{inu}}} \tag{26}$$

Applying the coordinate transformation of equations (25) and (26), equation (24) takes the following form:

$$\frac{\partial C_i}{\partial \hat{t}} + \hat{U}\frac{\partial C_i}{\partial \hat{x}} = Mw_{si}\left(F_i E_{si} - r_{0i}C_i\right) \tag{27}$$

where $\hat{U}$ denotes the apparent advection velocity in the transformed coordinate system, which takes the form

$$\hat{U} = \frac{1-\hat{x}}{\hat{t}} \tag{28}$$

The parameter M, which is a coefficient related to the model simplification and coordinate transformation, is defined as

$$M = \frac{R_{\mathrm{w}}}{UH\hat{t}\left(1-\hat{x}\right)} \tag{29}$$

This transformed coordinate system substantially reduces the magnitude of the advection term in equation (27) and thus the Courant number, so that the computational efficiency of the numerical scheme is significantly improved. However, equations (4)–(6), which relate to sedimentation from the tsunami, should not be solved in transformed coordinates, as this induces an apparent advective transport. Therefore, the value of C_i on computational grid points of the nontransforming coordinate system is estimated from the results of the numerical calculation of equation (27), using linear interpolation at each time step.

2.6. Model Implementation

We employed the finite difference method to obtain numerical solutions to our model. The parameters $\Delta\hat{t}$ and $\Delta\hat{x}$ are time and spatial steps used in the calculation. The model is coded in Python with modules NumPy and SciPy. Equation (27) is solved by the implicit Euler method. Then, equations (4)–(6) are solved by the predictor-corrector method with the two-step Adams-Bashforth scheme.

Boundary conditions are as follows:

$$C_i(\hat{x} = 0) = C_{0i} \tag{30}$$

$$C_i(\hat{x} = 1) = 0 \tag{31}$$

As the initial condition, the volume sediment concentration C_i of the ith grain size class is assumed to decrease linearly downstream:

$$C_i = C_{0i}(1-\hat{x}) \tag{32}$$

The initial grain size distribution in the active layer is taken to be uniform, so that F_i takes the same value regardless of i. Different choices for the initial grain size distribution such as the log-normal distribution do not affect the solution significantly.

As a result of the coordinate transformation, the balance equation of suspended sediment cannot be calculated when $\hat{t} = 0$ or $\hat{x} = 0$. Thus, the numerical calculation should be started at the time when the tsunami inundation flow has reached some location $x = x_0$. The initial value of $\hat{t}$ is then:

$$\hat{t}\big|_{x_{\max}=x_0} = \frac{x_0}{R_{\mathrm{w}}} \tag{33}$$

In this study, x_0 is set to 10 m, a value that is small enough to avoid grid dependence of the results. In the calculation, we set $\Delta\hat{x}$ and $\Delta\hat{t}$ equal to 0.01 and 0.001, respectively.

2.7. Test of the Forward Model

In order to test the forward model introduced here, a simulation is performed with a typical flow condition. The flow velocity U and the maximum inundation depth H are set to 2.5 m/s and 6.0 m, respectively. In this test,

the flow is *Fr* supercritical at the beginning of inundation. Froude number of the inundation flow decreases to the minimum value (0.32) at the seaward end of the calculation domain as the flow thickness increases, while it is still supercritical in the landward region even at the timing near the end of flow inundation. The sediment is discretized to four grain size classes (30, 88, 177, and 354 μm). The finest grain size class of sediment was set to 30 μm because mud particles in marine environment are generally flocculated, and the fall velocity of a characteristic floc aggregation is known to be equivalent to silt grains near 30 μm in diameter (Fildani et al., 2006). Sediment concentration at the upstream (seaward) boundary is set to 0.2% for 354 μm and 1% for other grain size classes in this simulation. The maximum inundation length is set to 3,000 m. Thus, the time to reach the maximum run-up point T_{inu}, which is calculated from the inundation length R_w divided by the flow velocity U, is 1,200 s.

The tsunami deposit produced by this simulation is characterized by a geometry that tapers downstream (landward), which is illustrated in Figure 3a. The deposit that forms during the run-up phase of the tsunami only occurs in the upstream (seaward) region, and the deposit during the stagnant phase drapes the inundated region with a landward linear decrease in thickness. A landward fining trend can be seen in the grain size distributions. The grain size distributions show lateral coarse-tail grading characterized by the selective removal of coarse-grained components (Figure 3b) (Branney, 1991). The coarsest component (354 μm) in the deposit is mostly found in the seaward region (0–500 m) (Figure 3c) with content rapidly decreasing downcurrent (landward). In contrast, the deposits containing the finest component (30 μm) extend until the landward end of the inundation limit (0–4,000 m), showing a linear decrease in thickness.

These characteristics of the thickness distribution reflect the spatial variation in the concentration of suspended sediment in the tsunami. The concentration of coarser grain size classes (354 and 177 μm) at the upstream (seaward) boundary exceeds the capacity of the flow to suspend it, and therefore, the concentration of these two size classes decreases downcurrent, resulting in deposition of a layer that shows rapid thinning downstream. After the concentration of these grain size classes have reached the equilibrium value at ~1,700 m from the upstream boundary, the suspended sediment concentration becomes constant in space. After this time during the flow run-up, all sediments bypassed the landward (downstream) region, so that no deposition occurred here. After the tsunami reached the landward (downstream) limit of the inundation, sediments of all grain size classes settle out. Sediments of finer grain size classes only deposit in this stagnant phase of the tsunami, and therefore the deposit in the stagnant phase of the tsunami shows a relatively wider range in grain size distribution in comparison to the deposit during the run-up phase. The deposit during the stagnant phase of the tsunami shows gradual changes in thickness along the entire inundation length, because the concentration of suspended sediment in the water column evolved to be was nearly spatially uniform, while flow depth linearly decreased inland.

2.8. Sensitivity of the Forward Model to the Variation of Model Parameters and the Choice of Model Assumptions

The numerical calculations of the forward model of tsunami deposits used in the FITTNUSS were conducted repeatedly to demonstrate the sensitivity of the model to input parameters and the selection of closure functions. First, the sensitivity of the forward model is examined by implementing the model with a variety of input parameters for run-up velocity U, maximum inundation depth H, and concentration C_i (Figure 4). Lower flow velocity induces higher concavity in thickness distribution and broader grain size distribution at the nearshore region, while the geometry of the tsunami deposits is nearly linear over a range of conditions corresponding to high flow velocity (Figure 4a). It is notable that the results at very high velocities (4.5–5.5 m/s) are quite similar, because the run-up flow can keep sediments of all grain size classes suspended over the calculational domain. In contrast to flow velocity, variation in the maximum inundation depth H does not affect grain size distribution of deposits significantly (Figure 4b). The inundation depth, however, is a critical parameter governing the thickness of the deposit (Figure 4b). The curvature of the thickness of the deposits also varied in accordance with inundation depth. The sediment concentration influences all properties of the tsunami deposits (Figure 4c). Both thickness and geometry of the tsunami deposit vary in response to changed sediment concentration. In particular, high-concentration flows result in thicker and more strongly concave deposits. The grain size distribution of deposits also varied depending on the initial sediment concentration. The deposit showed a broader grain size distribution at lower sediment concentration.

In addition to input parameters, the influence of the choice of the model assumption is examined here. The model assumption adopted in this study produces deposits showing intermediate characteristics

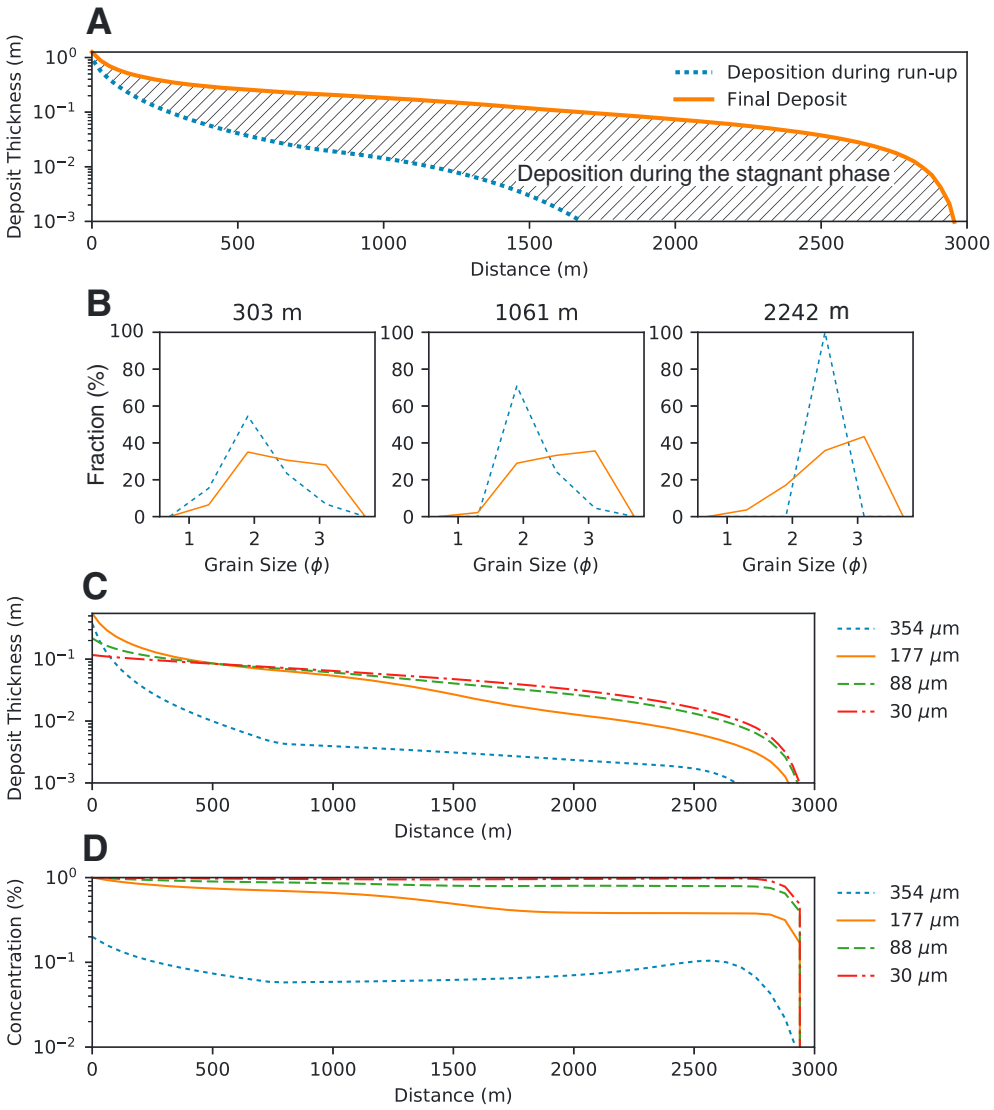

Figure 3. Result of sample calculation. Model parameters used in this calculation is as follows: $U = 2.5$ m/s; $H = 6.0$ m; Concentration of grain size class 354 μm is 0.2%; all other concentration values are 1%; $n = 0.03$; and $R_w = 3,000$ m. (a) Distribution of deposit thickness. (b) Grain size distributions of the deposit. (c) Volume of deposit per unit area of each grain size class. (d) Spatial variation of sediment concentration of each grain size class in the run-up flow when the flow has reached the maximum inundation point. See text for details.

between deposits corresponding to "no mixing" and "perfect vertical mixing" of suspended sediments by turbulence in the flow (Figure 5a). When there is no turbulent mixing in the flow (thus $r_{0i}C_i = C_0$) and no entrainment ($E_{si} = 0$) from the basal sediments, the suspended load in the run-up flow rapidly settles, producing a tapering geometry of the tsunami deposit (Figure 5). This no-turbulence assumption is nearly equivalent to the model of Soulsby et al. (2007). Under this model assumption, the coarsest fraction of suspension (354 μm) is lost within 300 m from the seaward end, producing very narrow grain size distributions in the region farther landward. In addition, the case "perfect vertical mixing" for which the vertical distribution of sediment concentration is uniform in the flow (thus, r_{0i} is unity) was also examined. This assumption corresponds to the situation in which turbulent mixing is extremely strong, and for which the loss of turbulence kinetic energy is not considered (thus, ψ_i in equation (19) is set to zero). In this case, all sediments are kept suspended in the flow, and the deposit shows a linear geometry (Figure 5). The grain size distribution of the deposit also becomes uniform. We also considered a third assumption, that is, a Rouse-type concentration profile without correction of turbulence damping effect by density stratification. This assumption resulted in deposits showing less concavity than the deposits resulting from the main assumptions used herein. Flows without

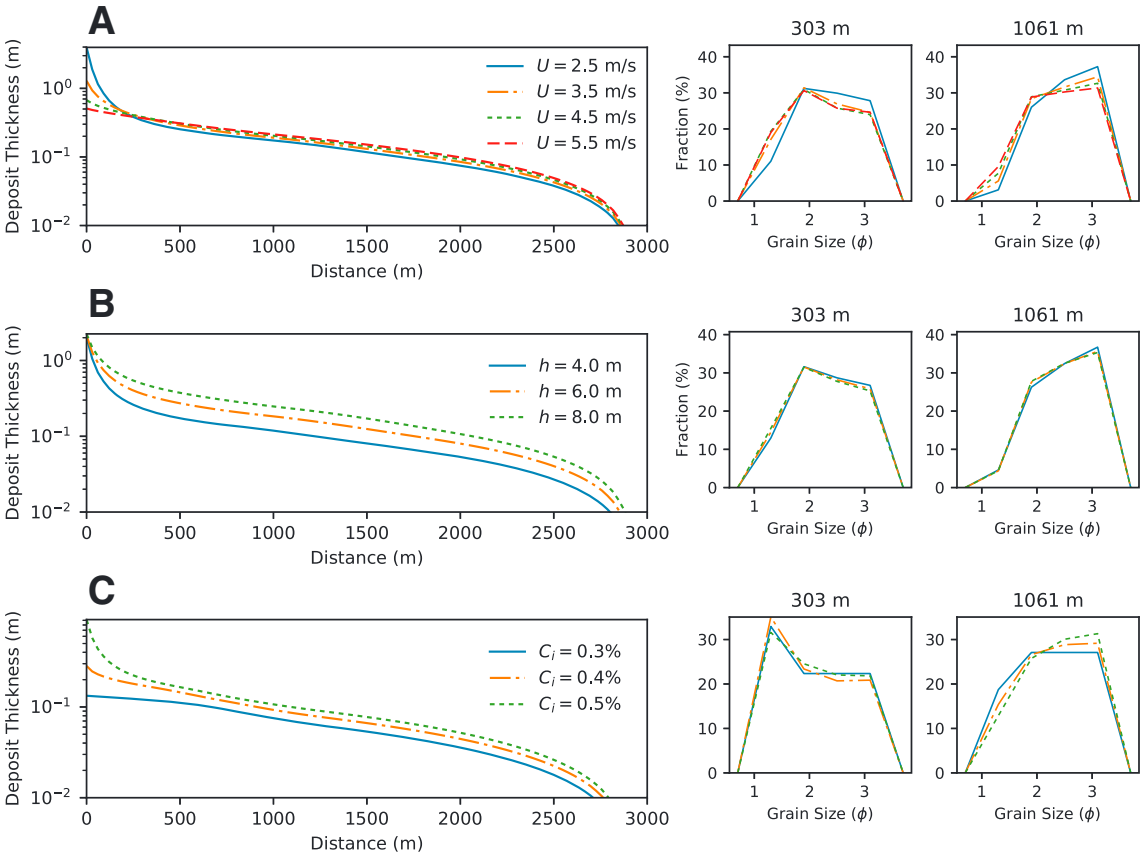

Figure 4. Sensitivity tests of the forward model against initial and boundary conditions. The variations of deposit thickness and grain size distribution at the locations 303 and 1,061 m landward from the upstream boundary are shown in these diagrams. Manning's n and the maximum inundation length R_w are fixed to 0.03 and 3,000 m, respectively. (a) Test against variation of flow velocity U. The other parameters used in this test are as follows: H_{max} = 6.0 m; Concentration of grain size class 354 μm is 0.5%; and all other concentration values are 1.0%. (b) Test against variation of maximum inundation depth H. The other parameters are as follows: U = 3.0 m/s; Concentration of grain size class 354 μm is 0.5%; and all other concentration values are 1.0%. (c) Test against variation of sediment concentration C_i. The other parameters are as follows: U = 3.0 m/s and H = 6.0 m.

turbulence damping can maintain larger amounts of sediment in suspension, so that this suspended sediment tends to bypass during the run-up phase of the tsunami. This results in deposits that show a more linear geometry in the stagnant phase.

Finally, the influence of variation of the model coefficients and empirical functions were investigated. Variation of the Manning's roughness coefficient n, which generally takes a range from 0.02 to 0.04 for the numerical simulation of tsunamis (Imamura et al., 2006), produces results that are almost equivalent to variation of flow velocity. The result obtained using a larger value of the Manning's n corresponds to that obtained with a higher velocity but with a correspondingly lower value of the Manning's n. A smaller value of the coefficient n makes the tsunami deposits thicker in the seaward (upstream) region and also slightly changes deposit thickness in the inland (downstream) region (Figure 5b). On the other hand, variation in thickness of the active layer L_a ranging from half to double the standard value is found to have negligible influence on thickness distribution of the tsunami deposits, although the grain size distribution in the nearshore region is slightly affected (Figure 5c). In comparison to other factors, variation in the sediment entrainment coefficient E_{si} has a strong effect on both thickness and grain size distributions of the deposits (Figure 5d). Values ranging from half to double the value obtained from the original equation of van Rijn (1984), as well as a value obtained from the sediment entrainment relation of Wright and Parker (2004) were tested here. The entrainment function of Wright and Parker (2004) takes the form

$$E_{si} = p\frac{AZ_{ui}^5}{1 + \frac{A}{0.3}Z_{ui}^5} \tag{34}$$

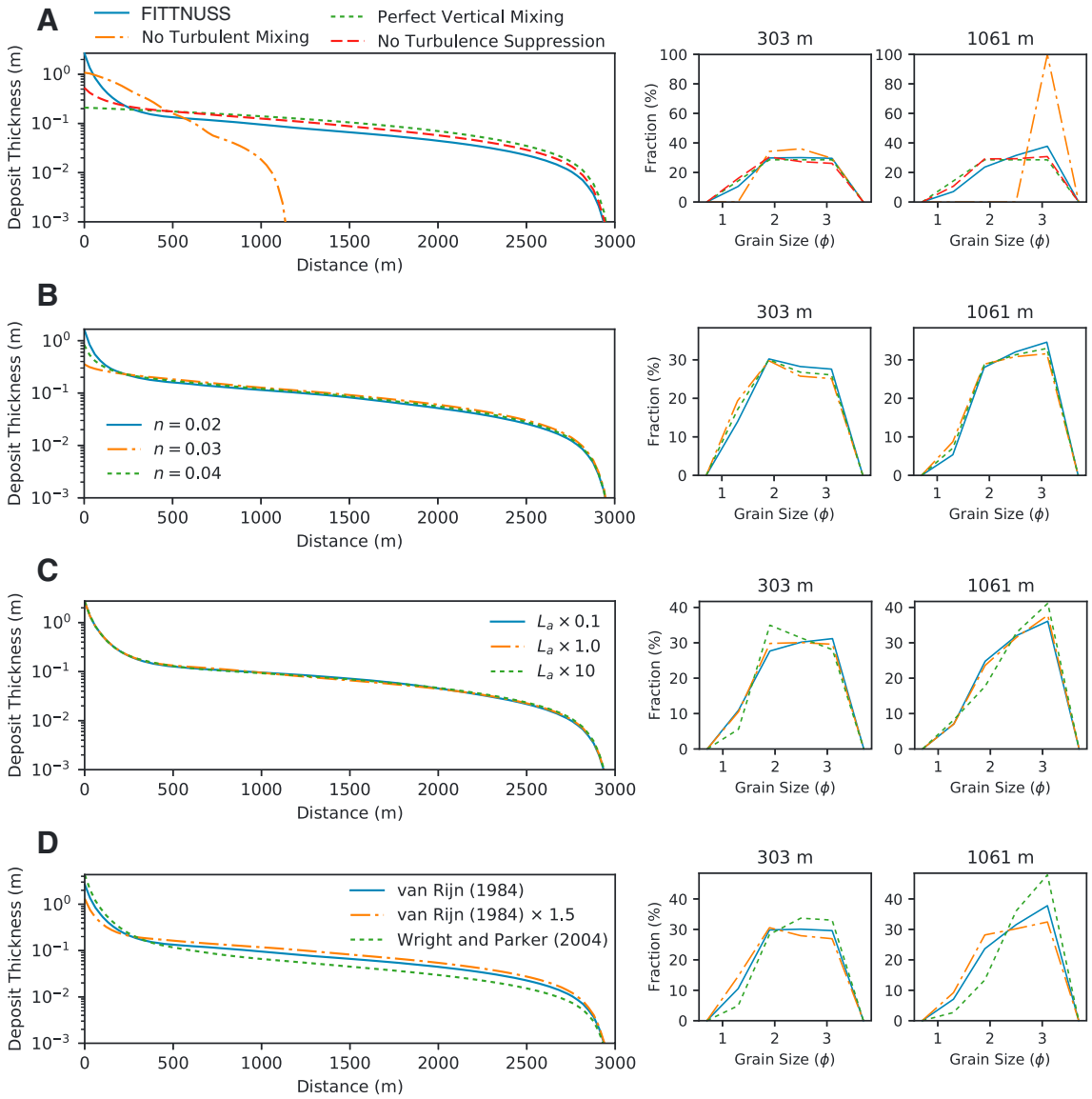

Figure 5. Sensitivity tests for dependency of results of the forward model on model assumptions and parameters. The variations of deposit thickness and grain size distribution at the locations 303 and 1,061 m landward from the upstream boundary are shown in these diagrams. The initial and boundary conditions used in these tests are as follows: $U = 3.0$ m/s; $H = 6.0$ m; Cocentration of the grain size class 354 μm is 0.3%; all other concentration values are 0.6%; $R_w = 3,000$ m. (a) Test for dependency of assumptions on turbulence and vertical distribution of suspended sediment. (b) Tests for selection of Manning's n values. (c) Tests for thickness of the active layer. (d) Tests for selection of sediment entrainment functions.

where A is an empirical coefficient ($= 7.8 \times 10^{-7}$) and

$$Z_{ui} = \frac{u_*}{w_{si}} Re_{pi}^{0.6} S_f^{0.08}. \tag{35}$$

Here S_f denotes friction slope, evaluated by

$$S_f = \frac{C_f U^2}{gh}. \tag{36}$$

and p is another empirical coefficient, which is set to 0.1 on the basis of Fildani et al. (2006). Calculations show that larger entrainment coefficients (E_{si}) produce more spatially uniform sediment concentrations in the flow, resulting in laterally extensive distributions of grain sizes within the deposits. The empirical function of Wright and Parker (2004) with the coefficient of Fildani et al. (2006) yields results that are about the same as those obtained with half of the coefficient of van Rijn (1984) at least under the conditions of this sensitivity test.

3. Inverse Modeling

Our model FITTNUSS conducts the inverse analysis of tsunami deposits by optimization of parameters used in the forward model. The inverse analysis estimates parameters corresponding to (1) the maximum inundation depth H, (2) the run-up velocity U, and (3) the sediment concentration of each grain size class C_i at the seaward (upstream) boundary of the study area (i.e., $\hat{x} = 0$). Measurements of the thickness and grain size distribution of the tsunami deposit, along with an estimate of the maximum horizontal run-up distance must be available for the inverse calculation. Procedures for conducting the inverse analysis of tsunami deposits are described below.

3.1. Data Preparation

In order to conduct the inverse analysis, the observed bed thickness η_{oj} and the volumetric fraction F_{oij} of each of the ith grain size classes of the tsunami deposit at the jth sampling site are converted to the form:

$$\eta_{oij} = F_{oij}\eta_{oj} \tag{37}$$

where $\eta_{oij}(x)$ denotes the volume per unit area of the ith grain size class of sediment at the jth sampling site. The volume per unit area η_{cij} of the ith grain size class of sediment at the jth sampling site is then obtained from the forward model calculation with the use of a cubic spline interpolation for $\eta_i(x)$.

3.2. Optimization of Objective Function

Here we define the inverse analysis of tsunami deposits in terms of minimization of the objective function Ψ specified below:

$$\Psi = \frac{\sum_i \sum_j \left(\eta_{oij} - \eta_{cij}\right)^2}{\sum_i \sum_j \eta_{oij}^2} \tag{38}$$

This objective function describes a bulk difference between the observed sediment volume per unit area of each grain size class and the corresponding value predicted from the numerical model. The parameter Ψ is expected to be minimized in the case for which the actual initial conditions are used in the forward model.

The optimization of parameters to minimize the objective function is performed using the limited memory Broyden-Fletcher-Goldfarb-Shanno method for bound-constrained optimization (the L-BFGS-B method). This method is an optimization algorithm in the family of quasi-Newton methods (Byrd et al., 1995). The L-BFGS-B method finds the optimized set of parameters using gradient of the objective function. The optimization is started from calculation of the forward model with the set of starting values of input parameters that are arbitrarily chosen, and the objective function is obtained from the result of the forward model. Then, calculations of the forward model with different input parameters are iterated in order to minimize the objective function on the basis of a gradient and Hessian of the function that are obtained numerically. Finally, the iteration of calculations is terminated when the decrease of the value in each step or gradient of the objective function at each iteration become lower than the predetermined value. The module SciPy of Python is used for this calculation.

The result of optimization can depend on the starting values (so-called initial guesses), so we employed the multiple start method in which the calculations of the optimization are started from multiple sets of initial parameters. As a result of optimization, different solutions can be obtained from different "initial guess" parameters, whereas most of solutions generally converge to the narrow range.

We adopted the best result from these multiple solutions. The correct answer cannot be obtained from arbitrary-starting values provided to the L-BFGS-B optimization method, because this quasi-Newton optimization method may find a local minimum solution of the objective function depending on the choice of the starting values. On the other hand, multiple solutions that can be regarded as nearly equivalent to the best solution may be obtained from different starting values. In this study, we set the criteria of the adoption of the solutions in accordance with (1) the objective function with a value lower than 1.0×10^{-7} or (2) deviation of the objective function by less than 1.0% from the best solution.

3.3. Test of the Inverse Modeling by Artificial Data

The inverse modeling FITTNUSS was evaluated by analyzing two series (totally eight sets) of artificial data that were produced by the forward model employed in this study. The first series of artificial data was created

Table 1
Results of the Inverse Analysis Using Artificial Data

	Maximum inundation length (m)	Run-up velocity (m/s)	Maximum inundation depth (m)	Characteristic diameters of grain size classes (μm)	Concentration of each grain-size class	Ratio of successful attempts of inversion	Starting Values producing best solution (U, H, Ci)
Case 1-1	3,000	2.50	6.00	177	1.0%	3.7%	(2.0 m/s, 7.0 m, 1.5%)
Case 1-2	3,000	2.50	6.00	88, 354	1.0%	51.9%	(4.0 m/s, 5.0 m, 1.5%)
Case 1-3	3,000	2.50	6.00	88, 177, 354	1.0%	59.3%	(4.0 m/s, 5.0 m, 1.5%)
Case 1-4	3,000	2.50	6.00	30, 88, 177, 354	1.0%	44.4%	(4.0 m/s, 7.0 m, 0.5%)
Case 2-1	5,000	5.00	8.00	177	1.2%	7.4%	(2.0 m/s, 5.0 m, 0.1%)
Case 2-2	5,000	5.00	8.00	88, 354	1.2%	3.7%	(2.0 m/s, 3.0 m, 1.5%)
Case 2-3	5,000	5.00	8.00	88, 177, 354	1.2%	11.1%	(4.0 m/s, 3.0 m, 0.1%)
Case 2-4	5,000	5.00	8.00	30, 88, 177, 354	1.2%	14.8%	(4.0 m/s, 3.0 m, 0.5%)

using 2.5 m/s for the flow velocity, 6.0 m for the maximum inundation depth, and 3,000 m for the maximum inundation length. The grain size distributions of sediments were discretized to single (177 μm), two (88 and 354 μm), three (88, 177, and 354 μm) or four (30, 88, 177, and 354 μm) grain size classes. The initial concentration of all grain size classes was set to 1.0%. The second series was created with 5.0 m/s for the flow velocity, 8.0 m for the maximum inundation depth, and 5,000 m for the maximum inundation length. Again, the grain size distributions of sediment were discretized to one to four grain size classes, each are similar to the corresponding one of the first series in diameter; concentration was set to 1.2% for all grain size classes. Values explored in this analysis range from 1.0 to 10.0 m/s for the run-up velocity, 2.0 to 14.0 m for the maximum inundation depth, and 0.01 to 5% for the sediment concentration. Starting values for optimization were chosen from combinations of: 2, 4, and 6 m/s for the flow velocity; 3, 5, 7, m for the inundation depth; and 0.1, 0.5, and 1.5% for the sediment concentration. For simplicity, the same values of initial concentrations were given as the starting values for all grain size classes. Thus, in total 27 combinations of the starting values were tested, and the best result, that is, the one that showed the smallest value of the objective function, was chosen as the result of the inverse analysis.

The best results were in all test cases found to match the true input values within ±0.1% in accuracy. When we define the criteria for the success of the inversion in terms of both (a) an objective function with a value lower than 1.0×10^{-7} and (b) reconstructed parameters that deviate by less than 1.0% from the true initial values in this test, it was found that the chance of success of the test varies remarkably in response to both the number of grain size classes and the initial conditions that were given to the forward models for creating test data sets (Table 1). As an overall trend, the tests of the first series in which relatively lower run-up velocities and inundation depths were adopted show higher chances of successful reconstruction of the input values. In cases using three or four grain size classes, the ratio of successful attempts of the inversion is fair (11.1 – 59.3%), implying that it is desirable to discretize the grain size distribution of sediment to more than three classes in order to succeed in inverse analysis. In contrast, the optimization method often failed to find the solution in the cases of single grain size class (3.7 – 7.4%). However, note that the best results in all cases always give accurate estimation of the input values (Table 1 and Figure 6).

4. Application to the 2011 Tohoku-Oki Tsunami Deposit

We applied our inverse model FITTNUSS to the 2011 Tohoku-Oki tsunami deposit for evaluation of the model. The tsunami deposit was examined along a transect transverse to the shoreline. The tsunami deposit was measured and sampled during a field survey conducted 3 months after the tsunami event. The results of our inverse analysis were verified by the observational data taken from aerial videos that included the moment of tsunami attack onto the Sendai Plain (Hayashi & Koshimura, 2013). Also, a reconstruction of the inundation depth of the tsunami was compared with the field data obtained by Mori and Takahashi (2012).

4.1. Field Description and Measured Data

We set a 4.02 km long transect from the shoreline to the inundation limit in the northern part of Sendai Plain (Figure 7). This transect is almost perpendicular to the shoreline. The survey region along the transect is mainly

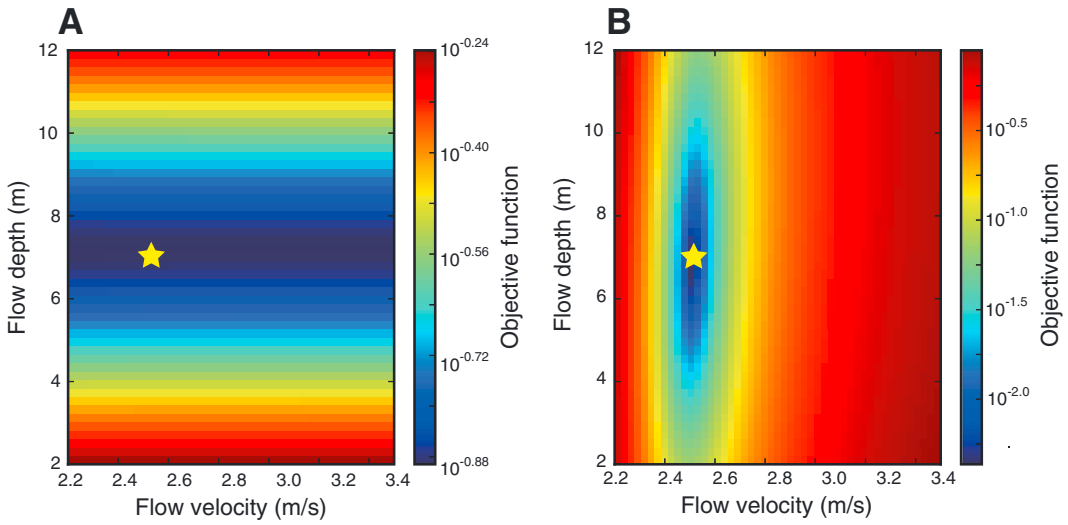

Figure 6. Distribution of values of the objective function for different input values of flow velocity *U* and flow depth *H*. The star-shaped symbols indicate the correct solution. Sediment concentration C_i was fixed to the value 0.3% that was used to produce the artificial data. (a) Distribution of the objective function in the test using uniform sediment (single grain size class). The objective function varies depending on the flow depth, while it is less sensitive to variation in flow velocity. (b) Distribution of the objective function in the test using the nonuniform sediment composed of four grain size classes. The objective function varies depending on both flow velocity and depth.

composed of the following topographies in landward order: (a) a 0.13 km long sandy beach, (b) a 6.2 m high onshore seawall, (c) a 2–3 m high aeolian sand dunes, (d) a 0.62 km long coastal forest of planted pine trees behind the beach, and (e) a low-lying zone of rice paddy fields that extends from 0.75 km to 3.93 km from the coastline (Figure 7).

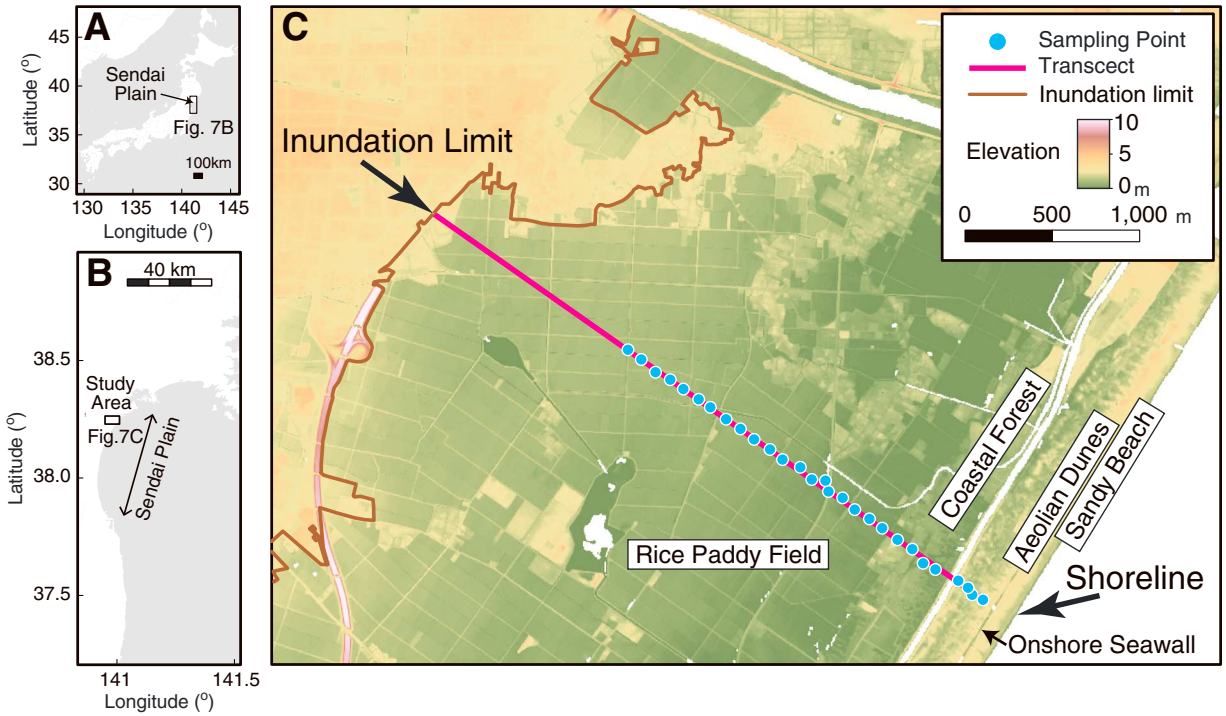

Figure 7. Location of the survey transect and sampling points on Sendai Plain. (a) Index map of Sendai Plain. (b) Location of the study area. (c) Topographic map of the study area and the location of the surveyed transect. The 4 km long transect was situated transverse to the shoreline, and the tsunami deposit was sampled at the 27 locations along the transect.

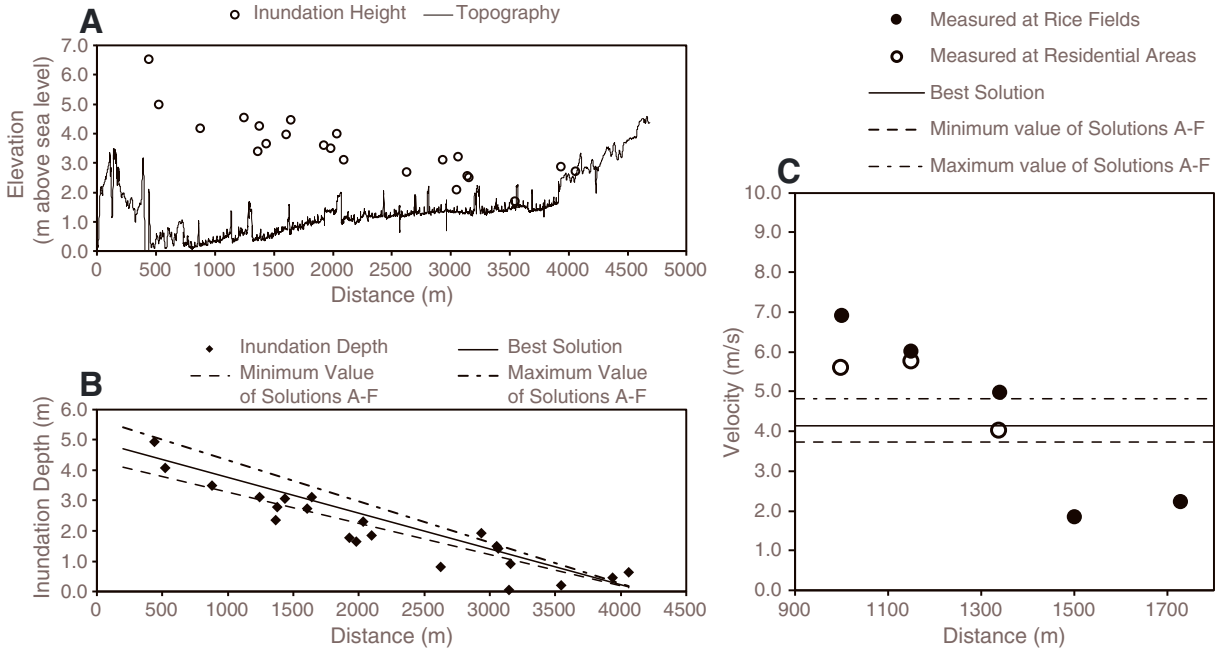

Figure 8. (a) Inundation heights of the 2011 Tohoku-Oki tsunami and topographic elevations above the mean sea level at Tokyo Bay measured by field observation along the transect. The topography was measured after the tsunami, so that it is affected by erosion or deposition by the tsunami. (b) Inundation depths of the 2011 Tohoku-Oki tsunami. The solid dots are measured values by field observation, and the lines are results of the inverse analysis of this study. (c) Velocity of run-up flow of the 2011 Tohoku-Oki tsunami on Sendai Plain. Values measured from the aerial videos are indicated by the solid and open circles, and the results of the inverse analysis are shown by the lines.

We surveyed the flow depth (flow height measured from the ground) and inundation limit along transects based on interviews of local people and field observations of watermarks. Data obtained by the 2011 Tohoku Earthquake tsunami Joint Survey Group were also used in this analysis (Mori & Takahashi, 2012). The tsunami inundated up to 4.02 km inland beyond the shoreline and 3.1 m above Tokyo Peil (TP, i.e., the mean sea level at Tokyo Bay) at the maximum (Mori & Takahashi, 2012) (Figure 8). The tsunami eroded the sand beach and aeolian dunes down to 2 m in the maximum depth, and transported large amounts of sandy sediment inland. The inundation height was 6.5 m above TP landward at the coastal forest and 3 m at a site 1.6 km from the shoreline; it further decreased inland (Figure 8). The average bed gradient between the point of inundation limit and the shoreline was 0.77×10^{-3}.

The flow velocities of the run-up flow of the 2011 Tohoku-Oki tsunami were measured from aerial video records of the Sendai Plain (1,000–1,800 m from the shoreline) (Hayashi & Koshimura, 2013). The velocity was 4.2 m/s on average, ranging from 1.9 m/s to 6.9 m/s (Figure 8).

The deposit of the transect for sampling and for the inverse analysis extended from the point at which the tsunami deposit showed maximum thickness to the point where the sand layer was pinched out (Figure 7). Erosional areas were excluded because the assumptions of the forward model are only valid in depositional areas. Along this transect, the deposit was sampled every 50–100 m, comprising 26 sites in total. The thickness of the tsunami deposit was measured using a scale at each site. The sand and mud layers deposited by the tsunami ranged from 0.1 cm to 34 cm in thickness, and were composed of fine to medium sand and 0.1–3 cm thick silt, respectively. Overall, sand thickness thinned and mud thickness gently thickened landward. The sand and mud thickness, however, fluctuated in association with local topography. The seaward boundary of the transect was located 0.1 km from shoreline, because the tsunami eroded the sandy beach of this region. In the region extending from 0.1 to 1.2 km from the shoreline, the tsunami deposit was composed of a 1–34 cm thick, medium-grained sand layer. Parallel laminations were occasionally observed in sand layers of this region. In the region extending from 1.2 to 3.0 km inland, the tsunami deposit ranged from 0.5 to 10 cm in thickness and was composed of fine- to medium-grained sand. The deposit was often draped by a 0.1–3 cm thick mud layer. In the region farther inland (3.0–4.0 km), the deposit thickness varied locally, showing a patchy distribution. Deposit thickness ranged from 0.1 to 0.3 cm, and the deposit was composed of massive fine- to medium-grained sand. It was commonly draped by a 1–3 cm thick mud layer.

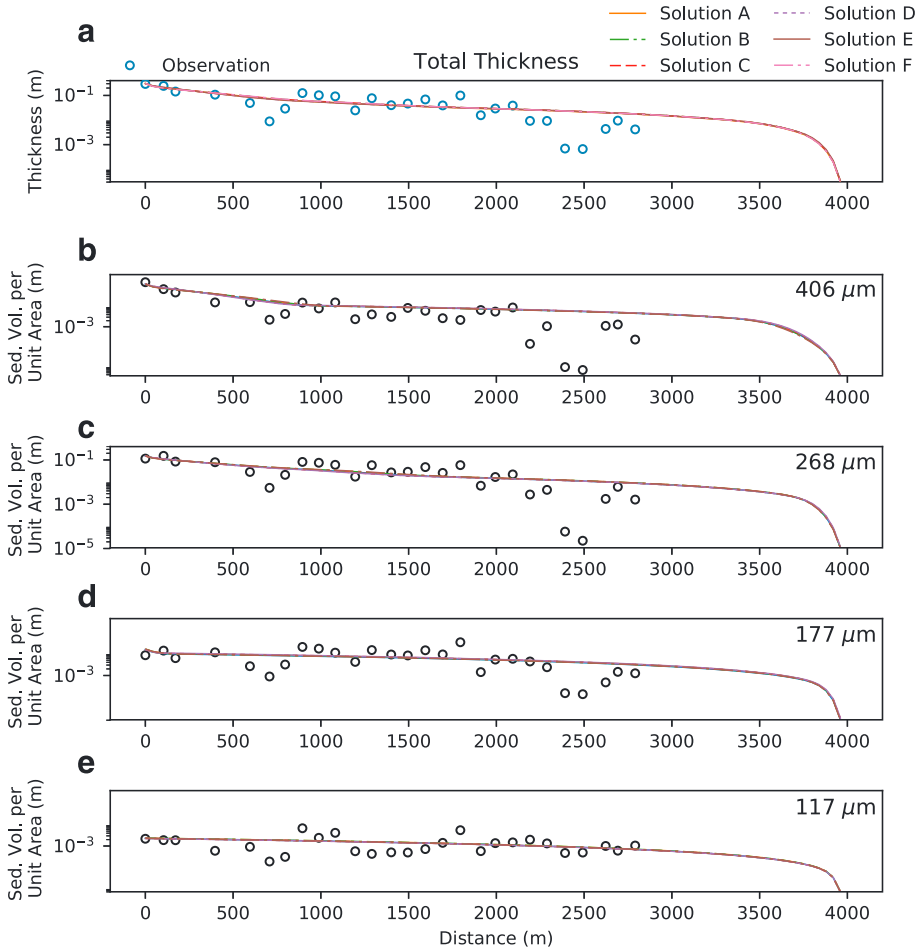

Figure 9. Spatial variation of thickness and grain size distribution of the 2011 Tohoku-Oki tsunami deposit along the transect. The open circles are values measured from the field survey in this study, and the lines indicate the results of the inverse analysis. (a) Spatial variation of thickness of the tsunami deposit. (b–e) Distribution of deposit volume per unit area of each grain size class.

Grain size analysis of the tsunami deposit revealed that the sand layer was composed mostly of medium sand with small amounts of fine and very fine sands (Figure 9). Mud and organic matter were removed from samples using a 0.063 mm mesh sieve, ultrasonic cleaning device, and 10% aqueous hydrogen peroxide. For grain size analysis, we used a 1.5 m long settling tube. Fractions of each grain size class were examined using the "Stube" application program (Naruse, 2005). Sediment particles from −1 to 4 ϕ were measured by the settling tube with 0.25 phi resolution. The measured grain size distributions were then discretized to four grain size classes (with the representative diameters 406, 268, 177, and 117 μm). The spatial variation of grain size distribution of the tsunami deposit was characterized by landward coarse-tail lateral fining, in which the coarsest fraction (medium sand) decreased exponentially in the landward direction, whereas the content of the finer fractions (fine and very fine sand) decreased landward linearly.

4.2. Result of the Inverse Analysis of the 2011 Tohoku-Oki Tsunami Deposit

As a result of the inverse analysis by FITTNUSS, a solution that can explain both the thickness and grain size distribution of the 2011 Tohoku-Oki tsunami deposit on the Sendai Plain was obtained (Figures 8 and 9; Table 2). This best solution corresponded to 4.15 m/s for the run-up velocity, 4.71 m for the maximum inundation depth at the first sampling site (203 m from the shoreline), and 0.36, 0.65, 0.13, and 0.03% for the concentration of suspended sediment of the four grain size classes, respectively. The total concentration of suspended sediments was 1.18%. Here we call this best solution as Solution A. The value of the objective function of Solution A was 1.626×10^{-1}. The run-up velocity of Solution A was very close to the spatial average of flow velocity

Table 2
Results of the Inverse Analysis of the 2011 Tohoku-Oki Tsunami Deposit on Sendai Plain

	Objective function	Run-up velocity (m/s)	Maximum inundation depth (m)	Sediment concentration at landward end				Starting values
				Total	406 μm	268 μm	177 μm	117 μm	(U, H, Ci)
Solution A	0.1626	4.15	4.71	1.18%	0.36%	0.65%	0.13%	0.03%	2.0, 5.0, 0.5%
	0.1626	4.15	4.71	1.18%	0.36%	0.65%	0.13%	0.03%	2.0, 7.0, 0.5%
	0.1626	4.15	4.71	1.18%	0.36%	0.66%	0.13%	0.03%	2.0, 5.0, 0.3%
	0.1626	4.15	4.71	1.18%	0.36%	0.65%	0.13%	0.03%	4.0, 5.0, 0.5%
Solution B	0.1629	4.00	5.00	1.13%	0.35%	0.63%	0.13%	0.03%	4.0, 5.0, 0.3%
	0.1630	4.00	5.00	1.13%	0.35%	0.63%	0.13%	0.03%	4.0, 5.0, 0.1%
Solution C	0.1632	4.51	4.34	1.28%	0.40%	0.70%	0.15%	0.03%	6.0, 7.0, 0.1%
Solution D	0.1637	4.69	4.20	1.32%	0.41%	0.72%	0.16%	0.03%	6.0, 7.0, 0.3%
Solution E	0.1640	3.72	5.40	1.05%	0.32%	0.59%	0.11%	0.03%	2.0, 5.0, 0.1%
Solution F	0.1641	4.81	4.10	1.35%	0.42%	0.74%	0.16%	0.03%	4.0, 3.0, 0.1%
	0.1650	5.06	3.91	1.42%	0.44%	0.77%	0.17%	0.03%	4.0, 3.0, 0.3%
	0.1652	5.11	3.85	1.43%	0.45%	0.77%	0.18%	0.03%	2.0, 3.0, 0.1%
	0.1652	5.15	3.87	1.44%	0.45%	0.78%	0.18%	0.03%	6.0, 5.0, 0.5%
	0.1658	5.34	3.79	1.48%	0.46%	0.79%	0.19%	0.04%	6.0, 7.0, 0.5%
	0.1662	5.49	3.71	1.52%	0.48%	0.81%	0.19%	0.04%	6.0, 5.0, 0.3%
	0.1662	5.51	3.70	1.52%	0.48%	0.81%	0.19%	0.04%	6.0, 5.0, 0.1%
	0.1673	6.11	3.47	1.63%	0.52%	0.86%	0.21%	0.04%	6.0, 3.0, 0.3%
	0.1673	6.12	3.47	1.63%	0.52%	0.86%	0.21%	0.04%	6.0, 3.0, 0.1%
	0.1673	6.13	3.46	1.64%	0.52%	0.87%	0.21%	0.04%	6.0, 3.0, 0.5%
	0.1685	3.21	6.49	0.88%	0.27%	0.50%	0.09%	0.01%	4.0, 7.0, 0.1%
	0.1689	8.76	2.85	2.00%	0.66%	1.03%	0.26%	0.05%	4.0, 3.0, 0.5%
	0.1690	3.18	6.59	0.87%	0.27%	0.50%	0.09%	0.01%	4.0, 7.0, 0.3%
	0.1693	10.00	2.73	2.14%	0.72%	1.09%	0.27%	0.05%	2.0, 3.0, 0.5%
	0.1693	10.00	2.73	2.14%	0.72%	1.09%	0.27%	0.05%	2.0, 3.0, 0.3%
	0.2487	2.00	7.00	0.48%	0.14%	0.32%	0.01%	0.01%	2.0, 7.0, 0.1%
	0.4179	10.00	6.31	1.10%	0.31%	0.65%	0.12%	0.02%	2.0, 7.0, 0.3%
	0.4179	10.00	6.49	1.07%	0.30%	0.63%	0.11%	0.02%	4.0, 7.0, 0.5%

measured from video records (Figure 8c). The inundation depth of Solution A was also found to fit to the observation (Figure 8).

However, in addition to the best solution described above, other solutions that also fit the observational data of the tsunami deposit on the Sendai Plain were obtained by the inverse analysis using multiple starting values (Table 2; Figure 9). When we set the criteria of the adoption of the solutions in accordance with deviation of the objective function by less than 1.0% from the best solution, five other solutions can be regarded as nearly equivalent to the best solution. Here we name these solutions as Solutions B to F (Table 2). Solutions B–F ranged from 3.72 to 4.81 m/s for run-up velocity, 4.10–5.40 m for maximum inundation depth at the first sampling site (203 m from the shoreline), and 1.05–1.35% for total concentration of suspended sediments. The estimated values of run-up velocity in these Solutions B–F were around the averaged value (4.2 m/s) of the observations (Hayashi & Koshimura, 2013). The inundation depths of these solutions were also found to fit the observations (Figure 8).

The influence of Manning's n on the results of inversion was also investigated (Table 3). Estimates of flow velocity varied remarkably from 6.05 to 3.08 m/s in response to the variation of n from 0.02 to 0.04. However, the variation of reconstructed values of inundation depth and sediment concentration in response to varied Manning's n was negligible. The inundation depth varied only from 4.70 to 4.74 m, and the sediment concentration was nearly constant (1.17 to 1.18% in total concentration).

Table 3
Best Solutions for Different Values of Manning's Roughness Coefficient n

Manning's n ($m^{-1/3}$ s)	Objective function	Run-up velocity (m/s)	Maximum inundation depth (m)	Sediment concentration at landward end					Starting values
				Total	406 μm	268 μm	177 μm	117 μm	(U, H, Ci)
0.020	0.1619	6.06	4.70	1.18%	0.36%	0.66%	0.13%	0.03%	2.0, 7.0, 0.3%
0.025	0.1624	4.89	4.70	1.18%	0.36%	0.66%	0.13%	0.03%	2.0, 7.0, 0.3%
0.030	0.1626	4.15	4.71	1.18%	0.36%	0.65%	0.13%	0.03%	2.0, 5.0, 0.5%
0.035	0.1628	3.52	4.73	1.17%	0.36%	0.65%	0.13%	0.03%	2.0, 3.0, 0.1%
0.040	0.1629	3.08	4.74	1.17%	0.36%	0.65%	0.13%	0.03%	2.0, 5.0, 0.5%

5. Discussion

5.1. Adequacy of the Forward Model

The forward model of tsunami sedimentation proposed in this study successfully reproduced typical characteristics of the tsunami deposits. Tsunami deposits generally span distances of several hundreds to thousands of meters inland (Morton et al., 2007) and gradually thin landward (Goto et al., 2014). The deposits varied in thickness largely in nearshore regions, but they formed a thin continuous veneer draping preexisting landforms farther inland. These features are well reproduced in the model presented here. In this model, the large variation of thickness in nearshore regions is attributed to deposition from overloaded suspended load transiting to bypassing conditions (Figure 3), and thus this part of the deposit is mainly formed during run-up of the tsunami. This prediction conforms with the observation that the modern tsunami deposits commonly show current-induced sedimentary structures such as lamination or rip-up mud clasts in nearshore regions (Naruse et al., 2010), but most thin layers farther inland regions lack these features, suggesting that they are deposits of suspension fall-out during the stagnant phase of the tsunami (Takashimizu et al., 2012). It is also frequently reported from observations and flume experiments that tsunami deposits fine inland (Fujino et al., 2008; Johnson et al., 2016). These features also coincide with the result of the forward model calculation in this study. More detailed comparison between the model and a modern deposit is provided based on the results of inverse analysis of the 2011 Tohoku-Oki tsunami deposit outlined in the next section.

In addition to the reproducibility of the modern tsunami deposits, the adequacy of the forward model can also be judged from its physical validity. Oversimplified models lacking physical bases may reproduce a specific observation with some calibrations, but it would not be applicable to a situation for which the model is not calibrated. Accurate physical validity while avoiding excessive computational cost is therefore significant for the inverse analysis, because the forward model is expected to be capable of prediction of the deposit accurately even the untested situations. Thus, the balance between computational costs and physical plausibility should be explored in regard to appropriate choices for inverse modeling.

The forward model used in the model FITTNUSS incorporates several physical processes such as deposition during the run-up, sediment entrainment and turbulence suppression due to density stratification (Cantero et al., 2012). Figure 5 illustrates the influences of the model assumptions on the predicted tsunami deposits. Although these processes are essential for predicting deposition from suspended load (van Rijn, 2007), they have not been fully considered in previous implementations of inverse analysis.

A sensitivity test of the forward model revealed that the model is sensitive to initial and boundary conditions (Figure 4), which suggests that the model is appropriate for inverse analysis. If the calculations resulting from different initial conditions does not vary significantly, it is difficult to estimate the initial condition from the consequence of the forward model. The flow velocity has especially strong influence to the results. This is probably because the entrainment rate of the suspended sediment changes according to the positive power of the flow velocity while the effect of the flow height on the thickness of the sediment is only a linear relationship. On the other hand, the inverse model needs to be robust to the model parameterization. Sensitivity analysis suggests that the results of our forward model calculation did not change significantly as a result of variation of the active layer thickness L_a (Figure 5). Variation of both the Manning's roughness coefficient n and the sediment entrainment coefficient E_{si}, however, were found to show considerable effects on the result (Figure 5).

5.2. Evaluation of the Test of the Inverse Analysis

The result of tests of the inverse analysis using FITTNUSS show that the method proposed in this study is capable of estimating the initial conditions of the tsunami deposits. The ratio of successful attempts from multiple start values increased when the number of grain size classes was increased to three or four. This is because the larger number of grain size classes adds more constraints to the model. Considering data noise and outliers in measurements of natural deposits, it is recommended to discretize grain size distribution of a measured tsunami deposit into three or more classes for model inversions.

The result of application of the inverse model to the tsunami deposit on the Sendai Plain was also successful. Except for several outliers in the measurement, the features of thickness and grain size distribution of the tsunami deposit are well fit by the calculated result using estimated parameters. Although optimized parameters did not converge to a single solution, but rather to multiple solutions that equivalently explain the data set, the solutions are all in the range of the observed data. Reconstructed values of run-up flow velocity are close to the spatial average of the measurements, and the estimations of the inundation depth are also close to the observations. It is difficult to evaluate the reconstructed values of sediment concentration because there are no observation data available. However, Goto et al. (2014) roughly estimated that sediment concentration in the inundation flow of the 2011 Tohoku-Oki tsunami was around 2% on the basis of relationship between thickness of deposits and inundation depths measured in various regions. Their estimation is not very far from the reconstructed concentration values of Solutions A–F, which range from 1.13 to 1.35%.

It is notable that there are limitations arising from the simplifications applied to the model. The reconstructed run-up velocity cannot explain the spatial variation of the flow velocity as measured by aerial video data, because the run-up velocity is simplified to be uniform in the model. Also, while the model predicts maximum inundation depth, it cannot satisfy spatial variations in flow depth which may occur in undulated topographic conditions because the model assumes that the slope of the water surface of the tsunami is both spatially and temporally constant. Nevertheless, the results of this study imply that reconstructed flow parameters such as the velocity and inundation depth obtained by the inverse analysis give averaged approximations of the field observation.

5.3. Comparison of Characteristics of the Present Inverse Model With Existing Models

Here we compare the characteristics of the inverse model proposed in this study with existing models. In comparison with existing models, our model FITTNUSS proposed in this study is expected to show a wider range of applicability than existing models, in part, because it encompasses transport of suspended sediment, which is spatially heterogeneously distributed, and deposition during both the run-up and stagnant phases of the tsunami. In addition to advective transport and sediment entrainment processes, the consideration of turbulent suppression due to density stratification is another innovative aspect of this model. Deposition during both run-up and stagnant phases of tsunamis are calculated, so that this model is suitable for both nearshore and inland areas and for both high- and low-velocity flows. The model does not require advance knowledge except for the inundation extent of the tsunami; as a result, it can apply to ancient tsunami deposits formed under relatively unknown conditions. Our model requires only a rather modest amount of input information. Knowledge of the spatial variation of both deposit thickness and grain size distribution, both of which can be measured only from the deposits, is required. Knowledge of the inundation extent of the tsunami is also a prerequisite for our model; but this as well can be estimated from the observed maximum inland extent of tsunami deposits (Koshimura et al., 2002; Nanayama et al., 2003). Indeed, the inverse version of this model successfully reconstructed the flow velocity and inundation depth of the 2011 Tohoku-Oki tsunami, one of the rare cases for which substantial data exist. Although the existing model TsuSedMod has also been used to successfully reconstruct flow conditions of the 2011 Tohoku-Oki tsunami (Jaffe et al., 2012), observation of the inundation depths and identification of the interval deposited in the stagnant phase were required as input to the analysis. For all inverse models, including our model, a bed roughness parameter such as Manning's n value must be calibrated for the given conditions of the bed; and the results of inverse analyses are inevitably sensitive to the bed roughness. In this study, n was set to 0.03 because it is a value commonly used for ricefield areas (Imamura et al., 2006). Estimation of flow velocity varied by nearly a factor of 2 when n was changed from 0.02 to 0.04 (Table 3). Nevertheless, range of variation of flow velocities estimated by our model was found to be relatively narrow in comparison with existing models such as TsuSedMod, whose estimates of flow velocity varied from 9.0 to 3.5 m/s when n is changed from 0.02 to 0.04. It is noteworthy that in our model, estimates of inundation depths were quite stable irrespective of choice of the n value.

5.4. Limitation of the Model

Even though our new inversion model FITTNUSS has a wide range of applicability, it has limitations due to the model assumptions. First, it can be applied only for the deposits on featureless plains without any significant built infrastructure or local topography variation. The influence of topography variation, which may be particularly important to the urbanized setting of Japan, on flow behavior is not considered in our model. For example, estuaries or regions near cliffs are not appropriate environments to use this method. The model FITTNUSS requires the maximum run-up length of tsunamis as one of the input parameters, which need to be estimated from the distribution of tsunami deposits or other evidence of tsunami inundation. Chagué-Goff et al. (2015) reported that the sandy tsunami deposit only reached 68% of the actual inundation limit in the lagoonal environment, suggesting that our method is not suitable for such topographically complicated region. On the other hand, many studies indicated that the limit of distribution of tsunami deposits reaches near the inundation limit on the flat coastal plains with abundant sandy sediment in source regions (Abe & Hori, 2016; Abe et al., 2012; Hori et al., 2007; MacInnes et al., 2009; Nakamura et al., 2012). Indeed, Szczuciński et al. (2012) indicated that the tsunami deposit contains sand fraction more than 5% even at the inundation limit on Sendai Plain. Thus, our model is suitable for the flat coastal plains and careful considerations about the sedimentary environments are recommended before applying the model FITTNUSS.

Study areas where slope significantly changes will violate the assumptions of the quasi-steady run-up flow analysis. Judging from the fact that our model well approximated the averaged flow velocity of the 2011 Tohoku-Oki tsunami, it seems that the quasi-steady assumption in our model can be justified in the region where the topography is smooth and nearly constant in slope. In addition, it is required that the study area should not be in a high-slope region where strong return flow occurs. Our model does not assume return flow, and therefore regions near topographic lows or channels are also unsuitable for our inverse analysis. Tsunami deposits near the shoreline often show multiple layers (Naruse et al., 2012). For analyzing such layered deposits, discrimination between deposits emplaced by run-up and return flows is needed before applying the inverse analysis, because our inverse model supposes only a single run-up flow followed by a stagnant phase.

5.5. Future Improvement—Framework for Inversion of the Tsunami Deposits

The model FITTNUSS proposed in this study provides a framework for inversion of the tsunami deposits. It is easy to implement new processes within it and to expand it for future studies. For example, there are various established methods for global optimization of objective functions, and advanced methods using evolution strategy will be targets for future implementation in our model. Available empirical functions for sediment entrainment are currently less reliable for very high velocity flows (e.g., >3.0 m/s), because there are few experimental results and observations for such conditions. A new sediment entrainment function based on experimental data for very high velocity flows will be implemented when it is available. Our model does not evaluate the vertical variation of grain size distribution in tsunami deposits; however, it would be easy to implement this feature because the forward model already has the ability to calculate the temporal evolution of grain size distribution. One of the most important issues for the improvement of our model is the incorporation of more advanced hydrodynamics of tsunamis. The transformed coordinate system used here is valid also for shallow-water equation systems in general (Kostic & Parker, 2006), so that the model can be amended to use the nonlinear long wave theory of tsunamis. The problem of computational costs may be addressed by using parallel computing.

Finally, the evaluation of uncertainty in estimation is an essential problem in this research field as pointed out by Jaffe et al. (2016). This study has revealed that the observed thickness and grain size distribution of the tsunami deposits can be reproduced by multiple sets of model input parameters. This is not a failure of the optimization method, but rather a limit of the information contained in the observations. The essential solution to the issue of narrowing the range of estimation is to acquire additional data from the deposits. Increasing sampling points and analysis of grain size distribution at high spatial resolution will improve the inversion results. Incorporation of geological observations such as sedimentary structures and recognition of the influence of local topography is an option to be incorporated in the inversion model. Information concerning bedforms could provide additional constraints on flow velocity and inundation depth. At the very least, they are useful to filter out unreasonable results from multiple solutions of the inversion problem. However, even if refinement of the forward model and the formulation of the objective function improves the results, it should not be expected that the results of the inversion would always converge to a single set of parameters, because (a) different processes can produce the same consequences and (b) deposits cannot provide a

complete record of the flow processes. Nevertheless, determining the degree of uncertainty in the inversion process is necessary in order to understand the limit of our knowledge, and to provide guidance as to the necessity of additional observation (Jaffe et al., 2016). Implementation of the cross validation or the bootstrap methods as well as data assimilation techniques such as Ensemble Kalman Filtering (EnKF) may help better quantify the uncertainty in future studies (Tang et al., 2016).

6. Conclusions

We propose a new model for the inverse analysis of tsunami deposits. Our inversion model FITTNUSS requires input data about the spatial variation of both thickness and grain size distribution of the tsunami deposit along 1-D shoreline-normal transects. It produces as output estimates of run-up flow velocity, maximum inundation depth and grain size-specific concentration of suspended sediment. The forward model of FITTNUSS calculates nonuniform sediment transport and deposition from tsunamis during both the run-up and stagnant phases. Processes related to suspended sediment transport such as turbulent mixing, sediment entrainment, and turbulence suppression due to density stratification are included in this model. A transformed coordinate system of moving boundary type is adopted in the model. This stabilizes the calculation and enhances computational efficiency. In the inverse analysis of the observed tsunami deposits, the L-BFGS-B method with multiple starting values is used for optimization of the parameters of the forward model. Tests of the inverse model using artificial data successfully reconstructed the original input values, illustrating the effectiveness of the optimization method employed in this study.

The new inversion model is applied to the 2011 Tohoku-Oki tsunami deposit on Sendai Plain, Japan. The thickness and grain size distribution of the tsunami deposit was measured along the 4 km long transect normal to the coastline. The best solution yielded the following values; 4.15 m/s for the run-up flow velocity, 4.71 m for the maximum inundation depth at the nearshore site (203 m from the shoreline), and 1.18% for the total sediment concentration. This results of the inversion were found to fit well to the velocities and inundation depths measured by aerial videos and field measurements. The successful analyses of both the artificial data and the actual tsunami deposits without any model calibration suggests wide applicability of our new model FITTNUSS. Our method is particularly suitable for the analysis of ancient tsunami deposits because it requires a minimum amount of information about the condition of tsunamis before reconstruction.

Notation

The symbols L, M, and T denote dimensions of length, mass, and time, respectively. The symbol [1] denotes that the value is dimensionless.

A Empirical coefficient of sediment entrainment function [1].
C Total layer-averaged sediment concentration [1].
C_i Layer-averaged sediment concentration of the ith grain size class [1].
C_f Bed friction coefficient [1].
C_q Sediment concentration in the active layer [1].
D_i Representative sediment diameter of the ith grain size class [L].
D_m Mean diameter of sediment in the active layer [L].
E_{si} Sediment entrainment coefficient [1].
F_i Volumetric fraction of the ith grain size class in the active layer [1].
H Maximum inundation depth of the tsunami at the seaward (upstream) boundary of the transect [L].
L_a Thickness of the active layer [L].
M Coefficient related to the coordinate transformation [$L^{-1}T$].
R Submerged specific density of sediment particles $= 1 - \rho_s/\rho_f$) [1].
R_w Maximum inundation length [L].
Re_{pi} Particle Reynolds number of the ith grain size class [1].
S Bed slope [1].
T_i Dimensionless bed-shear stress parameter [1].
T_{inu} Time to reach the maximum run-up point [T].
U Run-up velocity of the tsunami [LT^{-1}].
$\hat{U}$ Dimensionless run-up velocity [1].

Z_{ui} Parameter of the ith grain size class in the sediment entrainment relation [1].
a_1, a_2, a_3, a_4, a_5 Constants in the relation of sediment settling velocity [1].
b_1, b_2, b_3 Constants in the relation of the vertical profile of sediment concentration [1].
g Acceleration of gravity [LT^{-2}].
h Inundation depth of the tsunami [L].
n Manning's roughness coefficient [$L^{(-1/3)}T$].
r_{0i} Ratio of near-bed sediment concentration of the ith grain size class to layer-averaged concentration [1].
t Time [T].
$\hat{t}$ Dimensionless time [1].
u_* Friction velocity [LT^{-1}].
w_{si} Settling velocity of sediment of the ith grain size class [LT^{-1}].
x Bed-attached streamwise coordinate [L].
$\hat{x}$ Dimensionless bed-attached streamwise coordinate [L].
z Vertical coordinate [L].
Ψ Objective function to minimize a difference between observation and the forward model calculation [1].
η Thickness of the tsunami deposit [L].
η_i Volume per unit area of sediment of the ith grain size class [L].
θ Internal friction angle of sediment particles [1].
λ_p Porosity of the tsunami deposit [1].
μ Dimensionless settling velocity of sediment of the ith grain size class [LT^{-1}].
ν Kinematic viscosity of the water [L^2T].
ξ Dimensionless vertical coordinate $= z/h$ [1].
ρ_s Density of sediment particles [ML^{-3}].
ρ_f Density of the water [ML^{-3}].
τ_b Bed shear stress [$ML^{-1}T^{-2}$].
τ_{*m} Shields dimensionless shear stress using the mean grain size in the active layer [1].
ψ_i Coefficient in the relation of turbulent suppression due to density stratification [1].

Acknowledgments
The authors are deeply grateful to the Associate Editor Joel Johnson and the anonymous reviewer for their constructive comments to this article. The authors wish to thank Gary Parker of the University of Illinois at Urbana-Champaign for his helpful comments that greatly improved the manuscript. This work was partially supported by Japan Society for the Promotion of Science Grant-in-Aid for Scientific Research(B) grant JP26287127. Data of inundation height of the 2011 Tohoku-Oki tsunami are available at the web site of the 2011 Tohoku Earthquake tsunami Joint Survey Group (http://www.coastal.jp/tsunami2011/). All other data and source codes used in this paper are available at the first author's web site (http://turbidite.secret.jp/tsunami_deposit_inversion/).

References

Abe, T., & Hori, K. (2016). *Coastal geomorphology and tsunami disaster by the 2011 off the Pacific Coast of Tohoku earthquake*, Natural Disaster and Coastal Geomorphology (pp. 37–64). Switzerland: Springer.
Abe, T., Goto, K., & Sugawara, D. (2012). Relationship between the maximum extent of tsunami sand and the inundation limit of the 2011 Tohoku-oki tsunami on the Sendai Plain, Japan. *Sedimentary Geology*, *282*, 142–150.
Atwater, B. F. (1987). Evidence for great Holocene earthquakes along the outer coast of Washington State. *Science*, *236*(4804), 942–944.
Branney, M. J. (1991). Eruption and depositional facies of the Whorneyside Tuff Formation, English Lake District: An exceptionally large-magnitude phreatoplinian eruption. *Geological Society of America Bulletin*, *103*(7), 886–897.
Byrd, R. H., Lu, P., Nocedal, J., & Zhu, C. (1995). A limited memory algorithm for bound constrained optimization. *SIAM Journal on Scientific Computing*, *16*(5), 1190–1208.
Cantero, M. I., Cantelli, A., Pirmez, C., Balachandar, S., Mohrig, D., Hickson, T. A., … Parker, G. (2012). Emplacement of massive turbidites linked to extinction of turbulence in turbidity currents. *Nature Geoscience*, *5*(1), 42–45.
Chagué-Goff, C., Goff, J., Wong, H. K., & Cisternas, M. (2015). Insights from geochemistry and diatoms to characterise a tsunami's deposit and maximum inundation limit. *Marine Geology*, *359*, 22–34.
Choowong, M., Murakoshi, N., Hisada, K.-I., Charusiri, P., Charoentitirat, T., Chutakositkanon, V., … Phantuwongraj, S. (2008). 2004 Indian Ocean tsunami inflow and outflow at Phuket, Thailand. *Marine Geology*, *248*(3), 179–192.
Crank, J. (1984). *Free and moving boundary problems* (pp. 455). Oxford: Clarendon Press Oxford.
Dietrich, W. E. (1982). Settling velocity of natural particles. *Water Resources Research*, *18*(6), 1615–1626.
Fildani, A., Normark, W. R., Kostic, S., & Parker, G. (2006). Channel formation by flow stripping: Large-scale scour features along the Monterey East Channel and their relation to sediment waves. *Sedimentology*, *53*(6), 1265–1287.
Fujino, S., Naruse, H., Suphawajruksakul, A., Jarupongsakul, T., Murayama, M., & Ichihara, T. (2008). *Thickness and grain-size distribution of Indian Ocean tsunami deposits at Khao Lak and Phra Thong Island, Southwestern Thailand*. Tsunamiites–Features and Implications (pp. 123–132). Berlin: Elsevier.
Goff, J., Chagué-Goff, C., Nichol, S., Jaffe, B., & Dominey-Howes, D. (2012). Progress in palaeotsunami research. *Sedimentary Geology*, *243*, 70–88.
Goto, K., Hashimoto, K., Sugawara, D., Yanagisawa, H., & Abe, T. (2014). Spatial thickness variability of the 2011 Tohoku-oki tsunami deposits along the coastline of Sendai Bay. *Marine Geology*, *358*, 38–48.
Hayashi, S., & Koshimura, S. (2013). The 2011 Tohoku tsunami flow velocity estimation by the aerial video analysis and numerical modeling. *Journal of Disaster Research*, *8*(4), 561–572.
Hirano, M. (1971). River bed degradation with armoring. *Proceedings of Japan Society of Civil Engineers*, *1971*(195), 55–65.
Hori, K., Kuzumoto, R., Hirouchi, D., Umitsu, M., Janjirawuttikul, N., & Patanakanog, B. (2007). Horizontal and vertical variation of 2004 Indian tsunami deposits: An example of two transects along the western coast of Thailand. *Marine Geology*, *239*(3), 163–172.

Imamura, F., Yalciner, A. C., & Ozyurt, G. (2006). Tsunami modelling manual. (UNESCO IOC international training course on Tsunami Numerical Modelling). Retrieved from: www.tsunami.civil.tohoku.ac.jp/hokusai3/J/projects/ manual-ver-3.1.pdf

Jaffe, B., Goto, K., Sugawara, D., Gelfenbaum, G., & La Selle, S. (2016). Uncertainty in tsunami sediment transport modeling. *Journal of Disaster Research*, *11*(4), 647–661.

Jaffe, B. E., & Gelfenbaum, G. (2007). A simple model for calculating tsunami flow speed from tsunami deposits. *Sedimentary Geology*, *200*(3), 347–361.

Jaffe, B. E., Goto, K., Sugawara, D., Richmond, B. M., Fujino, S., & Nishimura, Y. (2012). Flow speed estimated by inverse modeling of sandy tsunami deposits: Results from the 11 March 2011 tsunami on the coastal plain near the Sendai Airport, Honshu, Japan. *Sedimentary Geology*, *282*, 90–109.

Johnson, J. P., Delbecq, K., Kim, W., & Mohrig, D. (2016). Experimental tsunami deposits: Linking hydrodynamics to sediment entrainment, advection lengths and downstream fining. *Geomorphology*, *253*, 478–490.

Kneller, B. (1995). Beyond the turbidite paradigm: Physical models for deposition of turbidites and their implications for reservoir prediction. *Geological Society, London, Special Publications*, *94*(1), 31–49.

Komar, P. D. (1985). The hydraulic interpretation of turbidites from their grain sizes and sedimentary structures. *Sedimentology*, *32*(3), 395–407.

Koshimura, S., Mofjeld, H. O., González, F. I., & Moore, A. L. (2002). Modeling the 1100 bp paleotsunami in Puget Sound, Washington. *Geophysical Research Letters*, *29*(20), 1948.

Kostic, S., & Parker, G. (2006). The response of turbidity currents to a canyon–fan transition: Internal hydraulic jumps and depositional signatures. *Journal of Hydraulic Research*, *44*(5), 631–653.

Kubo, Y., Masuda, F., Tokuhashi, S., & Sakai, T. (1998). Spatial variation in paleocurrent velocities estimated from a turbidite bed of the Mio-Pliocene Kiyosumi Formation in Boso Peninsula, Japan. *Journal of the Geological Society of Japan*, *104*(6), 359–364.

MacInnes, B. T., Bourgeois, J., Pinegina, T. K., & Kravchunovskaya, E. A. (2009). Tsunami geomorphology: Erosion and deposition from the 15 November 2006 Kuril Island tsunami. *Geology*, *37*(11), 995–998.

Minoura, K., Imamura, F., Sugawara, D., Kono, Y., & Iwashita, T. (2001). The 869 Jogan tsunami deposit and recurrence interval of large-scale tsunami on the Pacific coast of northeast Japan. *Journal of Natural Disaster Science*, *23*(2), 83–88.

Moore, A. L., McAdoo, B. G., & Ruffman, A. (2007). Landward fining from multiple sources in a sand sheet deposited by the 1929 Grand Banks tsunami, Newfoundland. *Sedimentary Geology*, *200*(3), 336–346.

Mori, N., & Takahashi, T. (2012). Nationwide post event survey and analysis of the 2011 Tohoku earthquake tsunami. *Coastal Engineering Journal*, *54*(1), 1–27.

Morton, R. A., Gelfenbaum, G., & Jaffe, B. E. (2007). Physical criteria for distinguishing sandy tsunami and storm deposits using modern examples. *Sedimentary Geology*, *200*(3), 184–207.

Nakamura, Y., Nishimura, Y., & Putra, P. S. (2012). Local variation of inundation, sedimentary characteristics, and mineral assemblages of the 2011 Tohoku-oki tsunami on the Misawa coast, Aomori, Japan. *Sedimentary Geology*, *282*, 216–227.

Nanayama, F., Satake, K., Furukawa, R., Shimokawa, K., Atwater, B. F., Shigeno, K., & Yamaki, S. (2003). Unusually large earthquakes inferred from tsunami deposits along the Kuril trench. *Nature*, *424*(6949), 660–663.

Naruse, H., Fujino, S., Suphawajruksakul, A., & Jarupongsakul, T. (2010). Features and formation processes of multiple deposition layers from the 2004 Indian Ocean Tsunami at Ban Nam Kem, southern Thailand. *Island Arc*, *19*(3), 399–411.

Naruse, H., Arai, K., Matsumoto, D., Takahashi, H., Yamashita, S., Tanaka, G., & Murayama, M. (2012). Sedimentary features observed in the tsunami deposits at Rikuzentakata City. *Sedimentary Geology*, *282*, 199–215.

Rouse, H. (1937). Modern conceptions of the mechanics or fluid turbulence. *Transactions of the American Society of Civil Engineers*, *102*(1), 463–505.

Soulsby, R. L., Smith, D. E., & Ruffman, A. (2007). Reconstructing tsunami run-up from sedimentary characteristics—A simple mathematical model. *Coastal Sediments*, *7*, 1075–1088.

Sugawara, D. (2014). Extracting magnitude information from tsunami deposits. *Journal of Geography (Chigaku Zasshi)*, *123*(6), 797–812.

Szczuciński, W., Kokociński, M., Rzeszewski, M., Chagué-Goff, C., Cachão, M., Goto, K., & Sugawara, D. (2012). Sediment sources and sedimentation processes of 2011 Tohoku-oki tsunami deposits on the Sendai Plain, Japan—Insights from diatoms, nannoliths and grain size distribution. *Sedimentary Geology*, *282*, 40–56.

Takashimizu, Y., Urabe, A., Suzuki, K., & Sato, Y. (2012). Deposition by the 2011 Tohoku-oki tsunami on coastal lowland controlled by beach ridges near Sendai, Japan. *Sedimentary Geology*, *282*, 124–141.

Tang, H., & Weiss, R. (2015). A model for tsunami flow inversion from deposits (TSUFLIND). *Marine Geology*, *370*, 55–62.

Tang, H., Wang, J., Weiss, R., & Xiao, H. (2016). TSUFLIND-EnKF inversion model applied to tsunami deposits for estimation of transient flow depth and speed with quantified uncertainties. *Marine Geology*. https://doi.org/10.1016/j.margeo.2016.11.009

van Rijn, L. C. (1984). Sediment transport, part II: Suspended load transport. *Journal of Hydraulic Engineering*, *110*(11), 1613–1641.

van Rijn, L. C. (2007). Unified view of sediment transport by currents and waves. II: Suspended transport. *Journal of Hydraulic Engineering*, *133*(6), 668–689.

Woodruff, J. D., Donnelly, J. P., Mohrig, D., & Geyer, W. R. (2008). Reconstructing relative flooding intensities responsible for hurricane-induced deposits from Laguna Playa Grande, Vieques, Puerto Rico. *Geology*, *36*(5), 391–394.

Wright, S., & Parker, G. (2004). Flow resistance and suspended load in sand-bed rivers: Simplified stratification model. *Journal of Hydraulic Engineering*, *130*(8), 796–805.

Yoshikawa, Y., & Watanabe, Y. (2008). Examine of Manning's coefficient and the bed-load layer for one-dimensional calculation of bed variation. *Monthly Report of Civil Engineering Research Institute for Cold Region*, *662*, 11–20.